A review on recently proposed oxime ester photoinitiators

Fatima Hammoud, Akram Hijazi, Michael Schmitt, Frédéric Dumur, Jacques Lalevée

A Review on Recently Proposed Oxime Ester Photoinitiators

Fatima Hammoud[1,2,3], Akram Hijazi[3], Michael Schmitt[1,2], Frédéric Dumur[4*] and Jacques Lalevée[1,2*]

[1] Université de Haute-Alsace, CNRS, IS2M UMR7361, F-68100 Mulhouse, France.

[2] Université de Strasbourg, France.

[3] EDST, Université Libanaise, Campus Hariri, Hadath, Beyrouth, Liban.

[4] Aix Marseille Univ, CNRS, ICR UMR 7273, F-13397 Marseille, France.

Corresponding authors: Frederic.dumur@univ-amu.fr; jacques.lalevee@uha.fr

Abstract:

This review is intended to highlight the recent developments and trends in the chemistry of oxime esters-based photoinitiators. It focuses on the mechanisms underlying the polymerization processes, measurement techniques, and various factors that affect the conversion efficiency. Due to their remarkable reactivities in photopolymerization reactions, oxime esters have attracted a great attention as reliable Type I (one-component) photoinitiators. In recent years, several research studies have been published with the purpose of modifying their chemical structures by introducing different chromophores or by varying the substitution pattern of the ester group, for which an interesting structure/reactivity/efficiency relationship could be achieved. In this review, an overview of the recent advances on oxime esters-based photoinitiators, as well as a comparison of the various scaffolds proposed in the literature is provided and discussed.

Keywords: Oxime esters, Type I photoinitiators, homolytic cleavage, photopolymerization, low light intensity, dyes, visible light

1. Introduction

Photochemical engineering of polymers and other modern materials science and technology has led to the creation of complex but effective methods for the fabrication of innovative materials, post-functionalization of polymers and novel synthetic products. [1-3] In these systems, light-activated chemical reaction pathways not only provide an excellent control over the reaction kinetics but also make it simple to carry out complex synthetic protocols. [4-7] Photoinduced polymerization systems may provide more flexible ways to synthesize macromolecules than polymerization systems induced by thermal, chemical, or electrochemical processes. As a result, recent advancements in these technologies have seen widespread being used in fields such as coatings, electronic circuits, digital storage, solar cells, and 3D precision machining. However, the majority of industrial polymerization processes currently under use relies on UV photoinitiating systems, which are facing a number of safety issues. [8-12] Actuality, the risk of UV radiation, which is the source of skin cancers and eye damages, as well as the formation of ozone during polymerization, are the main reasons that UV photopolymerization has been banned from some industrial applications and, more significantly, from consumer apps. High operating costs are also necessary because UV photopolymerization can only be done with pricey and energy-intensive setups. [13-15] The future of the planet now depends on reducing the energy consumption and improving the control of energy usage. Therefore, the search for more ecologically friendly polymerization processes is currently under progress.

Light-emitting diodes (LEDs) are a great choice for visible and secure light sources since these devices are compact and lightweight. LEDs have also low operating costs, long lifetimes, and low power consumption. In addition, these irradiation sources are now easily available. [16-18] In fact, efficiency of the electron transfer in multistep initiating procedures and the viscosity of the resins used to prepare the different photoinitiating systems are the unavoidable difficulties to deal with. At present, a wide range of two- or three component photoinitiating systems with absorption spectra perfectly matching the emission of LEDs are available. However, the complexity of the formulations can constitute a severe limitation for the future uses of these resins. In order to create more easily free radicals directly by the cleavage of chemical bonds, one-component type I PIs are now preferred. [19-22]

Only a few Type I photoinitiators, such as phosphine oxides and α-amino ketones, are currently compatible with near-UV and visible LEDs. The high reactivities of oxime esters (OXEs) as Type I photoinitiators in free radical photopolymerization are well known. In these structures, light irradiation can lead to the homolytic cleavage of the N-O bond, generating iminyl and

acyloxy radicals. The acyloxy radical is next subjected to a decarboxylation process, which results in the production of CO_2 and the formation of an active radical (See Scheme 1) which is quite similar to the known and proven Kolbe and Photo-Kolbe reaction. [22-27] It has to be noticed that during the photoinduced decomposition of oxime esters, only a nontoxic and nonhazardous gas is released within the photocurable resin, namely CO_2. Additionally, after decarboxylation reaction of aryloxy or acyloxy radicals, the probability of radical recombination with iminyl radicals is unfavorable so that aryl or alkyl radicals are more available for polymerization.

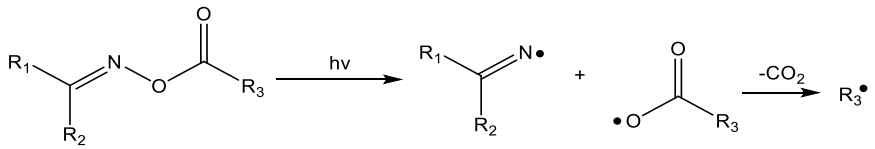

Scheme 1. Photochemical mechanisms involved in the decomposition of oxime esters. Reproduced with the permission from [47].

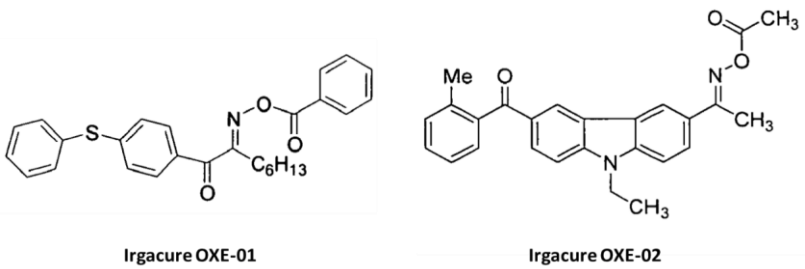

Scheme 2. Structures of commercial oxime ester photoinitiators OXE-01 and OXE-02.

O-Benzoyl-*α*-oxooxime (OXE-01) and *O*-acetyloxime (OXE-02) (Scheme 2), two commercial OXEs, are used to produce thick films for color filter resists. However, since OXE-01 and OXE-02's absorption bands were located in the UV range, these two oxime esters operate poorly if exposed to near-UV or visible LEDs. [28-30] Recently, a number of studies have been devoted to shift the oxime esters absorption wavelength into the visible range in order to better match their absorptions with the emission of various visible light sources. Different chromophores including coumarins, phenothiazines, triphenylamines, anthracenes, pyrenes, fluorenes and carbazoles were notably investigated during the last two years, evidencing the intense research activity in this field.

This review provides an overview of the different oximes esters recently developed by our groups at the Institute of Materials Science of Mulhouse (IS2M) and the Institute of Radical Chemistry (ICR) of Marseilles. Considering that numerous structures have been investigated, a comparison between the different families of chromophores is provided. Influence of the substitution pattern of the ester function on the photoinitiating ability of oxime esters is also discussed.

2. Triphenylamine based-oxime esters

Triphenylamine is a promising scaffold for the development of visible dyes. Triphenylamine is an electron donating group of low oxidation potential so that, when combined with an electron acceptor, push-pull dyes exhibiting an intense intramolecular charge transfer band extending over the visible range can be obtained. [31-32] The three-dimensional structure of triphenylamine also allows the corresponding dyes to significantly increase the solubility of the dyes produced compared to those made using its parent structure i.e. carbazole exhibiting a higher rigidity. Unlike carbazole, which has a planar structure that favors intermolecular interactions such as π-π staking, the three-dimensionality of triphenylamine is a real advantage to address the solubility issue. Aromatic rings of triphenylamine are excellent candidates for a variety of chemical modifications. Triphenylamine is particularly amenable to the majority of typical chemical reactions that form the core of Organic Chemistry. [33-35]

A series of triphenylamine-based oxime esters were investigated by Chen and coworkers in 2020 for their potential use as visible light photoinitiators. [36] In Scheme 4, chemical structures of four different triphenylamine-based Type I photoinitiators (**TP-1-TP-4**) and the synthetic route to access to these structures are shown. The synthetic protocols involve the following crucial steps: (1) a Buchwald-Hartwig C-N-coupling reaction to produce arylamines; (2) a Vilsmeier-Haack reaction to formylate the aromatic ring; (3) an oximation reaction of the aldehyde using sodium acetate as the base and hydroxylamine hydrochloride; and (4) a condensation reaction using benzoic anhydride in the presence of a base used as a catalyst to produce the desired compounds (**TP-1–TP-4**). UV-visible absorption spectra of the studied **TP-1-TP-4** compounds in CH_2Cl_2 are shown in Figure 1a, and Table 1 summarizes the different data. Absorption maxima of **TP-1-TP-4** were, respectively, 360, 364, 360 and 362 nm. Thus, the triphenylamine unit's substituted groups had a negligible impact on the max values. The emission spectra of each compound are shown in Figure 1 using an excitation wavelength of 360 nm.

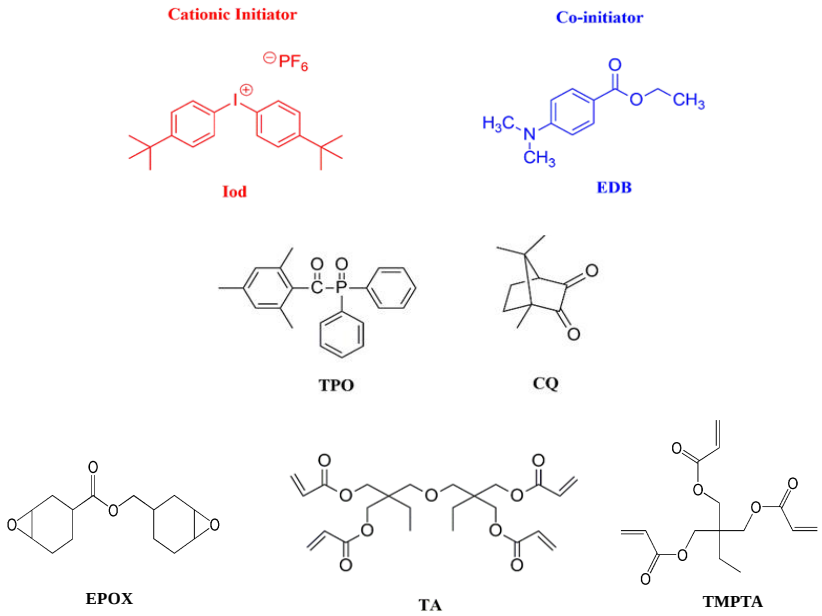

Scheme 3. Chemical structures of additives and monomers.

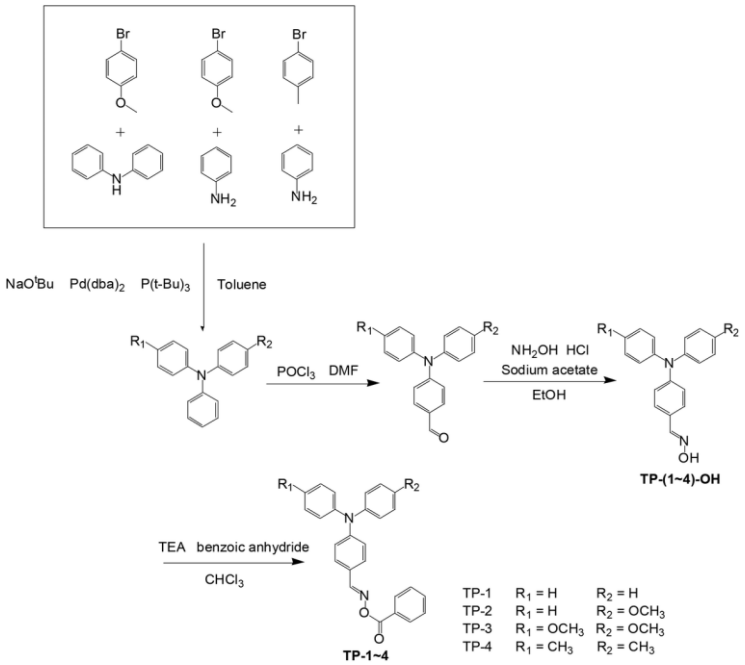

Scheme 4. Synthetic route to triphenylamine-based oxime esters (**TP-1**–**TP-4**). Reproduced with the permission from [36].

Photo-DSC profiles of all the newly developed photoinitiators are shown in Figure 2 and the results obtained during the photopolymerization experiments are gathered in Table 1. It's interesting to see how the photoreactivity of oxime esters is greatly influenced by the substitution introduced onto the triphenylamine core. According to the results obtained during the photopolymerization studies, the maximum heat flows and polymerization rates both decrease in the order **TP-1** = **TP-4** > **TP-2** > **TP-3** and **TP-1** = **TP-4** > **TP-2** > **TP-3**, respectively. Thus, **TP-1**, **TP-2**, **TP-3**, and **TP-4**'s final conversion efficiencies were determined as being of 92%, 74%, 78%, and 72%, respectively during the free radical polymerization (FRP) of trimethylolpropane triacrylate (TMPTA) (Scheme 3). Consequently, **TP-1**-**TP-4**-based photoinitiating systems exhibited excellent polymerization efficiencies. The formulation based on **TP-1** as the oxime ester furnished the best conversion efficiency of the series while using similar irradiation conditions. Steady state photolysis experiments carried out in DCM revealed **TP-1** to exhibit the fastest photolysis, supporting its remarkable photoinitiating efficiency.

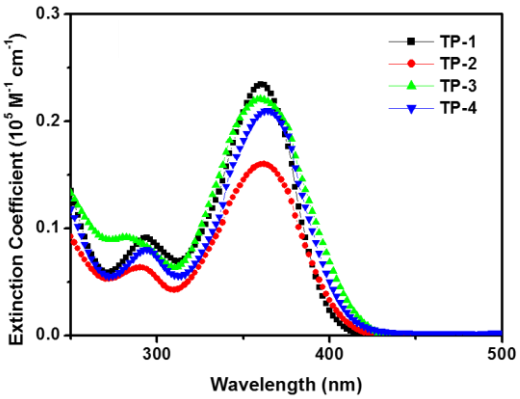

Figure 1. UV/Vis spectra of **TP-1**–**TP-4** in DCM solutions (Conc. = $1*10^{-5}$ M). Reproduced with the permission from [36].

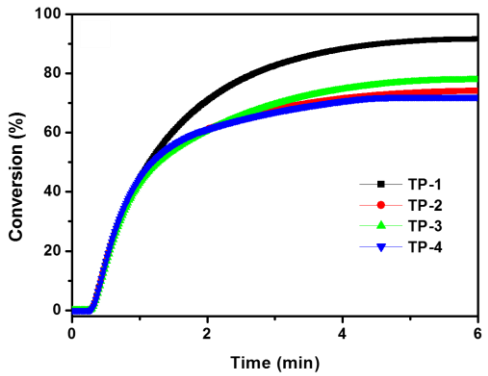

Figure 2. Conversion versus time of TMPTA photopolymerization initiated by **TP-1**–**TP-4** (2 wt%) under UV light irradiation. Reproduced with the permission from [36].

Table 1. Photo-DSC results derived from **TP-1–TP-4**.

Photoinitiators[b]	Final Conversion (%)	$H_{overall}$ (mW/mg)[c]	H_{max} (mW/mg)[d]	Rp_{max} (S^{-1})[e]	T_{max} (S)[f]
TP-1	91	79	66	89	25
TP-2	74	64	63	86	26
TP-3	77	67	61	84	27
TP-4	72	62	66	90	27

[a.] Measured with 80 W/m^2 of UV light for 6 min.
[b] Photo-DSC of the **TP-1–4**/TMPTA at weight ratios of **TP-1–4**: TMPTA = 2: 98
[c.] $H_{overall}$: overall heat flow values within 6 min.
[d.] H_{max}: maximum heat flow values.
[e.] Rp_{max}: maximum rate of polymerization.
[f.] T_{max}: time at maximum heat flow.

A more recent study from the same group proposed four new photoinitiators (PIs) (**TP-2p**, **TP-2m**, **TP-3m** and **Dml-m**) investigated for the free radical polymerization (FRP) of TMPTA, the cationic polymerization (CP) of (3,4-epoxycyclohexane)methyl-3,4-epoxycyclohexylcarboxylate (EPOX), and the elaboration of interpenetrated polymer networks (IPN), (see Scheme 5). As specificities, triphenylamine-based oxime esters comprise two or three oxime ester functions, enabling to tune the reactivity of OXE by mean of the number of photocleavable groups. [36] Synthetic procedures used to access to these structures include first (a) a formylation of the aromatic compound by mean of a Vilsmeier–Haack reaction; (b) an oximation reaction of the formyl group using sodium acetate as the base and hydroxylamine hydrochloride and (c) finally an esterification reaction of the oxime group with benzoic anhydride in the presence of triethylamine used as the base that could afford the different oxime esters in 70%, 90%, 70 and 60% yield respectively for **TP-2p**, **TP-2m**, **TP-3m** and **Dml-m**. These compounds showed an outstanding polymerization photoinitiation ability i.e. high polymerization rates and good final reactive function conversions, when irradiated with a LED@405 nm.

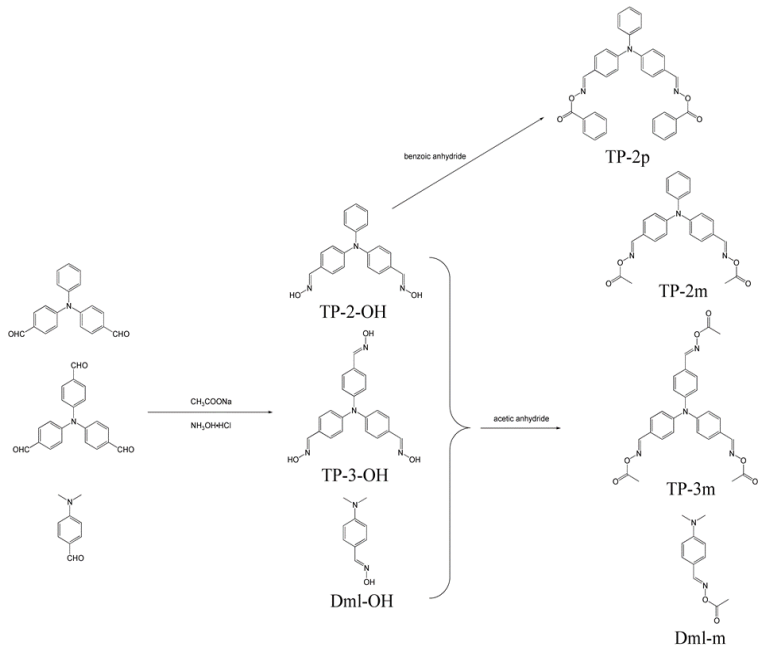

Scheme 5. Synthetic routes and chemical structures of the synthetized phenylamine-based oxime esters used in this research. Reproduced with the permission from Ref [37].

From the absorption point of view, **TP-2p**, **TP-2m**, and **TP-3m** showed mainly an absorption centered in the near UV range (300-425 nm), while **Dml-m** showed an absorption at a shorter wavelength (See Figure 3), highlighting the crucial role of the triphenylamine chromophore in red-shifting the absorption. **TP-3m** exhibited the highest molar extinction coefficient of the series due to the presence of three oxime ester functionalities in its structure, acting as electron withdrawing groups and increasing the electronic delocalization for this compound (See Figure 3).

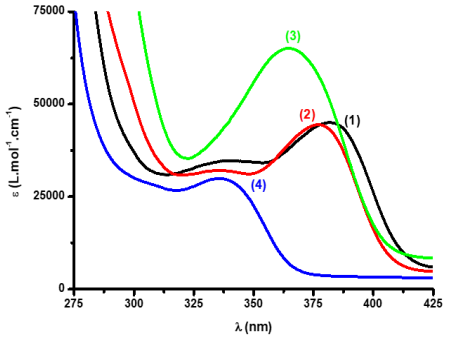

Figure 3. UV-visible absorption spectra of (1) **TP-2p**, (2) **TP-2m**, (3) **TP-3m** and (4) **Dml-m** in dichloromethane. Reproduced with permission of Ref. [37]

Considering their light absorption properties, all PIs were suitable to initiate the free radical photopolymerization (FRP) of TMPTA under LED@405 nm. Figure 4 displays typical acrylate conversion vs. irradiation time profiles. With the exception of **Dml-m**, all the examined OXEs exhibited high polymerization rates (See Figure 4(A, B); curve 4), which demonstrate the importance of the triphenylamine group in order to get a good absorbance at 405 nm in thin samples (25 µm in laminate) and in thick samples (1.4 mm under air) (see the light absorption properties above).

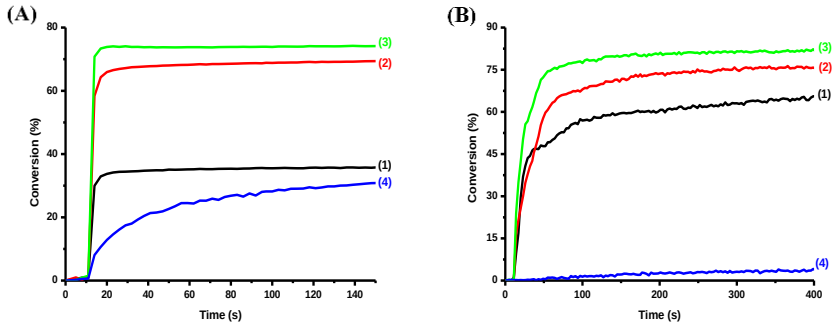

Figure 4. (A) Polymerization profiles of TMPTA (acrylate function conversion vs. irradiation time) in laminate (thickness = 25 µm) upon exposure to LED light λ= 405 nm in the presence of: (1) **TP-2p** (1% w); (2) **TP-2m** (1% w); (3) **TP-3m** (1% w); and (4) **Dml-m** (1% w); respectively. The irradiation starts after t = 10 s. (B) Polymerization profiles of TMPTA (acrylate function conversion vs. irradiation time) under air (thickness = 1.4 mm) upon exposure to LED light λ= 405 nm in the presence of: (1) **TP-2p** (1% w); (2) **TP-2m** (1% w); (3) **TP-3m** (1% w); and (4) **Dml-m** (1% w); respectively. The irradiation starts after t = 10 s. Reproduced with the permission from Ref [37].

Noticeably, polymerization efficiency of **TP-2p** was lower than that of **TP-2m** during the FRP of TMPTA at 405 nm. This is in stark contrast to the strong reactivity of the phenyl radical (produced in **TP-2p**), whose reaction rate toward the acrylate double bond is more than two orders of magnitude higher than that of the methyl radicals. This phenomenon was therefore assigned to the easier photocleavage of **TP-2m** upon irradiation as well as an easier decarboxylation process of **TP-2m** compared to **TP-2p** after homolytic cleavage of the N-O bond. However, since **TP-3m** has an additional oxime ester functionality in its structure, which can produce more radicals than the **TP-2m/ TP-2p series**, this OXE could furnish slightly higher conversions than **TP-2m** (See Figure 4).

The cationic polymerization of EPOX under LED illumination at 405 nm was also examined for the different afore-mentioned OXEs. Especially, the different OXEs were used as photosensitizers for an iodonium salt (Iod). Figure 5 displays the epoxy function conversion obtained vs. irradiation time curves upon irradiation at 405 nm. No polymerization occurred for Iod alone in EPOX, which is consistent with the lack of absorbance of Iod at 405 nm. Actually, the different OXEs can absorb light at 405 nm, and then the corresponding generated excited states of these compounds are expected to interact with Iod to generate the initiating species ($OXE^{\bullet+}$).

$$OXE\ (h\nu) \rightarrow {}^1OXE \qquad (r1)$$

$$^1OXE + Ar_2I^+ \rightarrow OXE^{\bullet+} + Ar^{\bullet} + ArI \qquad (r2)$$

Scheme 4. Mechanism involved in the polymerization process making use of two-component dye/Iod systems.

It has to be noticed that the photochemical reactivity of the different OXEs with the iodonium salt is certainly affected by the chemical structures of OXEs but also by differences of reactivity of the generated radical cations ($OXE^{\bullet+}$) formed by decomposition of the iodonium salt (See equation r2).

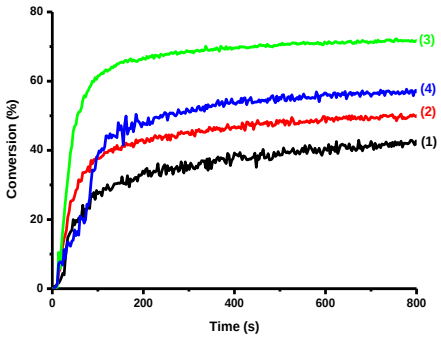

Figure 5. Polymerization profiles of EPOX (epoxy function conversion vs. irradiation time) under air (thickness = 25 µm) upon exposure to the LED light λ = 405 nm in the presence of: (1) **TP-2p**/Iod (1%/2% w/w); (2) **TP-2m**/Iod (1%/2% w/w); (3) **TP-3m**/Iod (1%/2% w/w); and (4) **Dml-m**/Iod (1%/2% w/w); respectively. The irradiation starts after t = 10 s. Reproduced with the permission from Ref [37].

Furthermore, it was suggested to combine radical and cationic polymerizations in order to create interpenetrating polymer networks (IPN) that would have the benefits of both techniques without the drawbacks. Table 5 provides a summary of the final acrylate and epoxy function conversions obtained upon irradiation at 405 nm for 800 s. The experimental findings demonstrate that the OXE/Iod systems can induce the hybrid polymerization for a combination of 50% wt TMPTA and 50% wt EPOX (See Table 5). Noticeably, in thin films, the acrylate conversion was greatly higher than that of the epoxides, attributable to the higher reactivity of the phenyl radicals compared to the $OXE^{\bullet+}$ radical cations. Conversely, under air, an opposite situation was found, with EPOX conversions on par with that of TMPTA. It can be confidently assigned to oxygen inhibition, adversely affecting the FRP of TMPTA. Indeed, the CP of epoxides being insensitive to oxygen inhibition, higher monomer conversions can be obtained under air compared to that obtained in laminate.

Parallel to the photochemically induced polymerization processes, all OXEs also exhibited an excellent thermal initiating ability. By differential Scanning Calorimetry (DSC), a maximum exothermicity was determined at 155°C, with an onset temperature of 115°C. As shown in the Figure 6, the highest exothermicity was observed for the trifunctional oxime ester i.e. **TP-3m**, furnishing a monomer conversion of 65%. Following **TP-3m**, the best TMPTA conversions were obtained for the difunctional OXEs **TP-2m** and **TP-2p**, with monomer conversions of 60 and 42% respectively. It can be thus concluded that in the case of the thermal

activation, increase of the number of reactive functions drastically improves the monomer conversion.

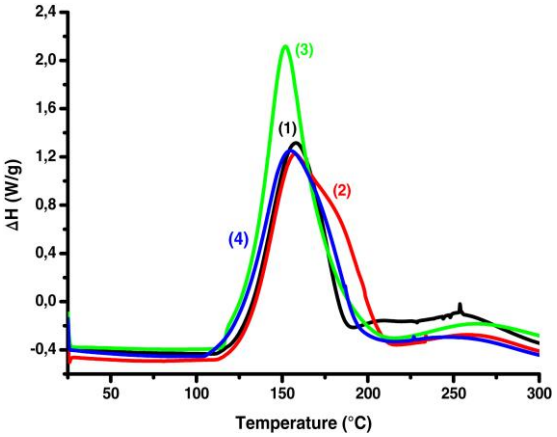

Figure 6. Thermal polymerization (enthalpy vs. heating temperature) of TMPTA determined at a heating rate of 10 K/min, under nitrogen. (1) 1% **TP-2p**, (2) 1% **TP-2 m**, (3) 1% **TP-3 m**, and (4) 1% **Dml-m**. Reproduced with the permission from Ref [37].

Table 5. Final acrylate or epoxy function conversion (FCs) for the polymerization of a TMPTA/EPOX blend (50%/50% w/w) using different two-component OXE/Iod (1%/1% w/w) photoinitiating systems after 800 s of irradiation with a LED (λ = 405 nm).

	Thin sample (25 µm) in laminate		Thick sample (1.4 mm) under air	
	Acrylate function	Epoxy function	Acrylate function	Epoxy function
TP-2p/Iod	77%	26%	43%	42%
TP-2m/Iod	89%	14%	39%	36%
TP-3m/Iod	94%	16%	38%	29%
Dml-m/Iod	69%	26%	51%	21%

Overall, the new series of OXE could efficiently initiate the CP of EPOX and the FRP of TMPTA, as well as the synthesis of interpenetrated polymer networks in which the concomitant polymerization of EPOX and TMPTA can be obtained. Based on their light absorption characteristics, cleavage ability, decarboxylation reaction, and the reactivity of the produced radicals, some pertinent structure/efficiency relationships could be examined. Interestingly, these OXEs could display a dual thermal and photochemical initiating ability, and to the best

of our knowledge, this is the first time that this dual activation mode was demonstrated for oxime esters. This dual ability is of crucial importance, especially when a thermal activation is needed for polymerization in dark areas. In this case, the dual activation mode may offer up an additional curing opportunity in addition to the photochemical one.

3. Coumarin based-oxime esters

As chromophores commonly used for the development of Type II photoinitiators, coumarins, which are present in a variety of bacteria, fungi, and edible plants, have received a specific attention starting from 2019 for the design of oxime esters. [38-40] Indeed, if highly efficient photoinitiating systems could be prepared with coumarins, the only way to get high monomer conversions consisted in using three-component systems. The first coumarin-based oxime esters were reported in 2018 by Liu and coworkers with aim at simplifying the composition of the photocurable resins. [41,42] Unimolecular photoinitiators are currently actively investigated due to the easiness to handle. Indeed, research done recently on oxime esters has amply demonstrated that the efficiency of oxime ester's polymerization was correlated with two key factors: first, the effectiveness of the photocleavage, and second, the capacity of decarboxylation of acyloxy or aryloxy radicals. Recent studies in this area have shown that even if an efficient photocleavage could take place, the inability of aryloxy radicals to evolve into aryl radicals had a significant impact on the monomer conversion. Aryloxy radicals do, in fact, react with acrylic monomers less strongly than aryl radicals. By detecting the release of CO_2 in the reaction media at 2337 cm^{-1}, infrared spectroscopy makes it particularly simple to monitor the absence of decarboxylation and which species is involved in the polymerization process.

In 2021, an interesting study has compared the reactivity of different radicals produced by decarboxylation, the nature of the radicals formed having a significant impact on the polymerization efficiency.[43] This study aimed at comparing ten different oxime esters comprising the same chromophore (namely a coumarin) but exhibiting different substituents on the ester side. Among all OXEs proposed in this work, **OXE-B**, **OXE-C** and **OXE-H** (See Scheme 5) have previously been reported in the literature. [29,41,42] All oxime esters could be obtained in high yields, as shown in Scheme 6.

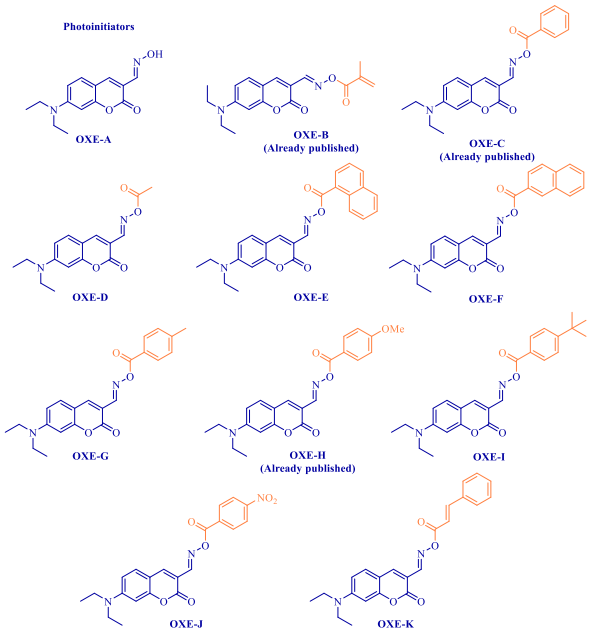

Scheme 5. Chemical structures of the synthetized coumarin-based oxime esters used in Ref [42].

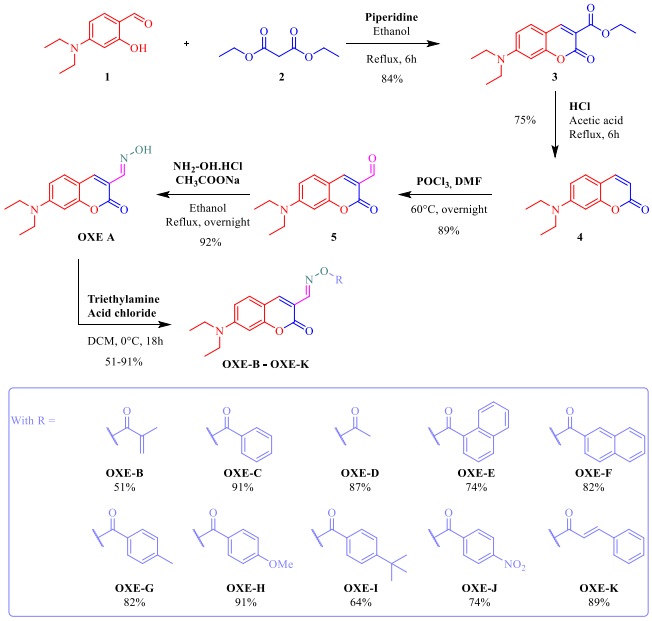

Scheme 4. Synthetic routes to **OXE-B-OXE-K**.

OXE-B-**OXE-K** exhibited broad absorption spectra with nearly identical absorption maxima, as listed in the Table 6. Esterification of the oxime group in **OXE-B**-**OXE-K** resulted in a 20 nm redshift of the absorption maxima compared to that of the parent **OXE-A**, namely a non-esterified oxime (λ_{max} = 418 nm). As a result of this, absorption maxima ranging from 431 nm for **OXE-B** and **OXE-D** up to 441 nm for **OXE-J** could be determined by UV-visible absorption spectroscopy. In this series of oxime esters, **OXE-J** (ε = 50 000 $L.mol^{-1}.cm^{-1}$) bearing the strongest electron-withdrawing group on the ester i.e. a nitro group exhibited the highest molar extinction coefficient. All dyes had short excited-state lifetimes that ranged from 1.58 ns for **OXE-I** to 1.92 ns for **OXE-B**. Thus, it can be concluded that the singlet state constitutes the primary deexcitation pathway.

Table 6. Light absorption properties of the investigated compounds; maximum absorption wavelengths (λ_{max}), extinction coefficients at λ_{max} and extinction coefficients at 405 nm.

PI	λ_{max} (nm)	ε_{max} ($M^{-1}cm^{-1}$)	$\varepsilon_{(405nm)}$ ($M^{-1}cm^{-1}$)
OXE-A	418	28000	25500
OXE-B	431	33000	22000
OXE-C	436	40500	23500
OXE-D	431	34000	22500
OXE-E	437	28500	16500
OXE-F	437	36000	21000
OXE-G	436	31500	18000
OXE-H	435	26500	17000
OXE-I	437	37000	20500
OXE-J	441	50000	25000
OXE-K	435	31000	18000

According to the results obtained during the photopolymerization tests using **OXE-A**-**OXE-K** in TMPTA under 405 nm irradiation, **OXE-J** provided the highest final monomer conversion (73%), followed by **OXE-D** (72%) (See Figure 7). As anticipated, **OXE-A**, which is not an oxime ester, had the lowest monomer conversion. In this case, a TMPTA conversion as low as 34% was determined after 150 s of irradiation. Surprisingly, **OXE-H**, which has been previously reported in the literature, had the worst monomer conversion of the series of oxime esters. In TMPTA, a monomer conversion as low as 42% was calculated. For all the other oxime esters, monomer conversions ranging between 52 and 61% were obtained. Considering the diversity of monomer conversions obtained for a series of oxime esters bearing the same

chromophore for light absorption, it therefore evidenced the crucial role of the group used to esterify the oxime moiety.

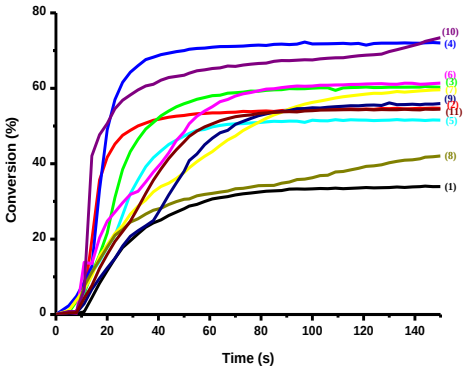

Figure 7. Photopolymerization profiles of TMPTA (acrylate function conversion vs. irradiation time) in laminate (thickness = 25 µm) upon exposure to LED light λ = 405 nm in the presence of: (1) **OXE-A** (0.5% w); (2) **OXE-B** (0.5% w); (3) **OXE-C** (0.5% w); (4) **OXE-D** (0.5% w); (5) **OXE-E** (0.5% w); (6) **OXE-F** (0.5% w); (7) **OXE-G** (0.5% w); (8) **OXE-H** (0.5% w); (9) **OXE-I** (0.5% w); (10) **OXE-J** (0.5% w); and (11) **OXE-K** (0.5% w); respectively. The irradiation starts after t = 10 s. Reproduced with the permission from Ref [42]

Given that the absorption characteristics of all oxime esters are comparable, differences of their polymerization speeds depend on other factors such as the efficiency of the photocleavage reaction, the efficacy of the decarboxylation reaction, and the reactivity of the produced radicals. All of these variables are crucial to the photopolymerization processes. By calculating the bond dissociation energies (BDE) of all oxime esters, this point could be further explored. According to Table 8, values for **OXE-B** and **OXE-J** ranged from 42.31 kcal/mol and 50.58 kcal/mol, respectively. For the enthalpy of decarboxylation $\Delta H_{decarboxylation}$, more notable differences could be evidenced.

Only **OXE-D** was able to conduct a photoinduced decarboxylation reaction that was energetically favorable ($\Delta H_{decarboxylation}$ = E(R$^{\bullet}$) + E(CO_2) - E(RC(=O)O$^{\bullet}$) = - 4.94 kcal/mol). Thus, the determined highly favorable decarboxylation mechanism for **OXE-D** is consistent with the measured polymerization features. With the appearance of a peak at 2337 cm^{-1} during the polymerization of TMPTA, Fourier Transform Infrared spectroscopy (FTIR) could evidence the occurrence of a decarboxylation process (See Figure 8). The absence of a CO_2 peak during photopolymerization for all the other oxime esters indicated a low decarboxylation

yield. Reactivity of the radicals (R•) once created is another crucial factor. Indeed, once formed, radicals should add onto the C=C double bond but be not too reactive towards formation of midchain radicals (MCRs) and/or backbiting, hydrogen transfer. [43] Radical reactivity can be anticipated by analyzing the spin density on the radical center, in this case, carbon-centered radicals. Thus, an improvement of the free radicals reactivity is obtained when the spin is more localized. Too much localization can affect stability and reduce selectivity. Here again, **OXE-D** was discovered as having the highest spin density, demonstrating the extraordinary reactivity of this oxime ester.

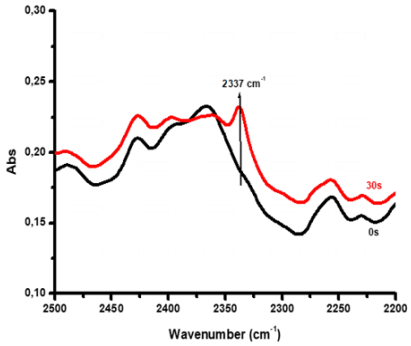

Figure 8. Detection of CO_2 release during the polymerization with **OXE-D**. Reproduced with permission of Ref [42].

Theoretical calculations further showed that the photocleavage step proceeded from the singlet excited state rather than from the triplet excited state due to the unfavorable enthalpy of cleavage (See Table 8).

Table 8. Parameters characterizing the investigated OXEs. Some parameters characterizing the proposed oxime esters were calculated by molecular modelling: the Bond Dissociation Energy BDE (N-O), the triplet state energy E_{T1}, the enthalpy $\Delta H_{cleavageT1}$ for cleavage process from T_1, the enthalpy $\Delta H_{decarboxylation}$ for decarboxylation reaction and the spin density. The singlet excited state energy E_{S1}, the enthalpy $\Delta H_{cleavageS1}$ for cleavage process from S_1, and the fluorescence lifetime of the OXEs were measured experimentally.

PI	BDE (N-O) (kcal.mol^{-1})	E_{S1} (kcal.mol^{-1})	$\Delta H_{cleavage\ S1}$ (kcal.mol^{-1})	τ_0 (S1) (ns)	E_{T1} (kcal.mol^{-1})	$\Delta H_{cleavage\ T1}$ (kcal.mol^{-1})	$\Delta H_{decarboxylation}$ (kcal.mol^{-1})	Spin density ($R^{\bullet}$)
OXE-A	64.56	61.8	2.76	3.36	42.70	21.86	-	-
OXE-B	42.31	59.72	-17.41	1.92	47.49	-5.18	0.52	0.999
OXE-C	48.42	59.26	-10.84	1.65	44.67	3.75	5.92	0.989
OXE-D	48.87	60.42	-11.55	1.89	44.83	4.04	-4.94	1.156

OXE-E	45.54	59.49	-13.95	1.64	44.74	0.8	4.36	0.999
OXE-F	48.34	59.26	-10.92	1.61	44.60	3.74	6.24	0.995
OXE-G	48.14	59.03	-10.89	1.65	44.61	3.53	6.92	0.990
OXE-H	47.85	58.57	-10.72	1.79	44.51	3.34	8.77	0.996
OXE-I	48.13	59.49	-11.36	1.58	44.61	3.52	6.97	0.989
OXE-J	50.58	-	-	-	44.78	5.8	3.14	0.998
OXE-K	49.09	59.72	-10.63	0.989	44.42	4.67	7.64	1.076

Parallel to their investigations as Type I photoinitiators, their photoinitiating ability as Type II photoinitiators was also examined when used as photosensitizers for the sensitization of an iodonium salt given that all oxime esters contain the same chromophore i.e. the coumarin unit. When combined in two-component OXE/Iod (0.5%/1% w/w) systems for the FRP of TMPTA upon irradiation at 405 nm, all OXE demonstrated higher photoinitiating abilities in two-component OXEs/Iod systems (higher polymerization rates and higher final conversions) than considered alone (See Figure 9). In two-component systems, it was possible to establish the following reactivity order: **OXE-J** > **OXE-D** > **OXE-C** > **OXE-A** > **OXE-G** > **OXE-H** > **OXE-F** > **OXE-B** > **OXE-K** > **OXE-I** > **OXE-E**. In this case, no CO_2 signal could be seen in the FTIR spectra when utilized as photosensitizers for the decomposition of the iodonium salt, irrespective of the dyes. Notably, no CO_2 signal was detected for **OXE-D** when used as Type II photoinitiators whereas this peak was clearly detectable for **OXE-D** used as type I photoinitiator. These results are indicative that the electron transfer from the coumarin unit towards the iodonium salt was faster than the photocleavage of the oxime esters.

The authors suggested a classical process from a mechanistic point of view. Thus, an electron transfer between the excited dye and the iodonium salt may take place upon irradiation, causing the oxidation of the excited dye and decomposing the iodonium salt as aryl radicals Ar• (See Scheme 4).

Commenté [DF1]: Il manque une figure visiblement. D'ailleurs, c'est Scheme 5, pas 4

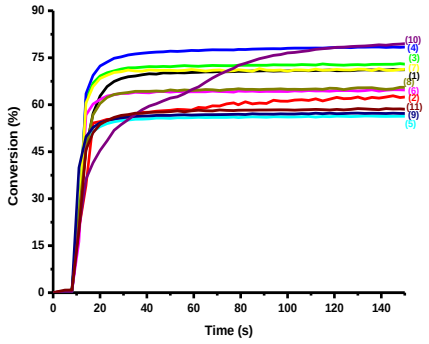

Figure 9. Photopolymerization profiles of TMPTA (acrylate function conversion vs. irradiation time) in laminate (thickness= 25 µm) upon exposure to LED light λ = 405 nm in the presence of: (1) **OXE-A**/Iod (0.5%/1% w/w); (2) **OXE-B**/Iod (0.5%/1% w/w); (3) **OXE-C**/Iod (0.5%/1% w/w); (4) **OXE-D**/Iod (0.5%/1% w/w); (5) **OXE-E**/Iod (0.5%/1% w/w); (6) **OXE-F**/Iod (0.5%/1% w/w); (7) **OXE-G**/Iod (0.5%/1% w/w); (8) **OXE-H**/Iod (0.5%/1% w/w); (9) **OXE-I**/Iod (0.5%/1% w/w); (10) **OXE-J**/Iod (0.5%/1% w/w); and (11) **OXE-K**/Iod (0.5%/1% w/w); respectively. The irradiation starts at t = 10 s. Reproduced with permission of Ref [42].

Due to the strong reactivity of **OXE-D**, direct laser write experiments could be carried out to create 3D structures. As shown in Figure 10, the two-component **OXE-D**/Iod (0.1%/1% w/w) system enabled the creation of 3D patterns with a high spatial resolution in a relatively little amount of time (within two minutes) using (oxy*bis*(methylene))*bis*(2-ethylpropane-2,1,3-triyl)tetraacrylate (TA) as the monomer.

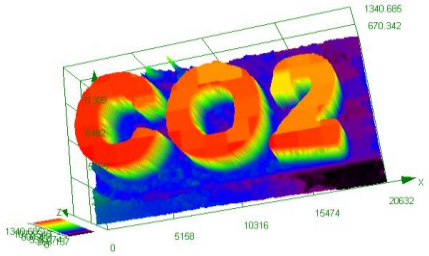

Figure 10. Optical microscopy of the 3D patterns obtained using the two-component **OXE-D**/Iod (0.1%/1% w/w) system in a TA, upon exposure to a laser diode @405 nm. Reproduced with permission of Ref [42].

Finally, the possibility to induce a thermal cleavage of the different oxime esters was examined. Indeed, investigation of the thermal cleavage of oxime esters remains scarce in the literature. Significantly, **OXE-D** once again demonstrated a high efficiency as a thermal initiator compared to the others. Polymerization of TMPTA could begin at temperatures as low as 155°C (See Table 10). **OXE-D** can therefore function as a powerful photoinitiator for both

photochemical and thermal reactions. In particular, the generation of Me$^{\bullet}$ radicals, which are the highly reactive radicals for initiating polymerization processes, is closely correlated with the high reactivity of **OXE-D**.

4. Carbazole based-oxime ester

Due to its polyaromaticity, the planarity of its structure enabling carbazole to exhibit a high thermal and photochemical stability, its excellent electron-donating ability as well as its good solubility in most monomers, carbazole has been identified as a promising scaffold for the design of photoinitiators. Carbazole is an inexpensive starting material that can be used to create economical Type I photoinitiators. It can also be easily chemically modified. [44-47] During the last three years, no less than a hundred photoinitiators based on carbazole have been reported in the literature. Several carbazole-based oxime esters have been reported by our group at the Institute of Materials Science of Mulhouse (IS2M).

As photoinitiators for visible light photopolymerization, a series of Type I photoinitiators (PIs) based on the nitrocarbazole scaffold have been developed and tested for the first time in 2021. [48] Originally, three oxime esters (**OXE-M**, **OXE-V**, and **OXE-P**) with different terminal groups attached via the oxime ester group (acetyl, acryloyl, and benzoyl) were synthesized (See Scheme 6). In this work, the nitrocarbazole scaffold was considered as an appropriate structure for the design of visible light photoinitiators. Indeed, absorption of carbazole is strongly UV-centered and carbazole do not naturally absorb in the visible range. To address this issue, introduction of a nitro group enabled to get the desired absorption in the visible range while facilitating the purification. Indeed, the nitro group is well-known to reduce the solubility of dyes so that the different oxime esters could be purified by a simple precipitation with ether.

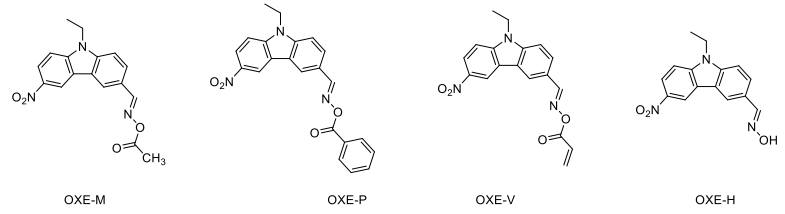

Scheme 6. Chemical structures of the nitrocarbazole-based oxime esters **OXE-M**, **OXE-V**, **OXE-P** and **OXE-H**.

As anticipated, the substitution pattern of the oxime ester group had no influence on the absorption maxima of all dyes, for which absorption maxima were detected at 376 nm. This is

consistent with the chromophore moiety centered onto the carbazole unit and not on the oxime substituent. Due to the existence of an extra aromatic ring over **OXE-M** (ε = 13 000 $M^{-1}.cm^{-1}$) and **OXE-V** (ε = 12 400 $M^{-1}.cm^{-1}$), **OXE-P** was found to have the highest molar extinction coefficient (ε = 13 800 $M^{-1}.cm^{-1}$). In order to conduct the polymerization studies at 405 nm, molar extinction coefficients of 4100, 3900, and 4100 $M^{-1}.cm^{-1}$ were found at this wavelength. In fact, photolysis of oxime esters was monitored in real time, which revealed a new peak at 2337 cm^{-1}. These experiments successfully proved that CO_2 was released during irradiation.

As anticipated, **OXE-H** did not produce any CO_2 during irradiation as this molecule is not esterified and this compound was thus unable to initiate a decarboxylation reaction. The energy of bond dissociation could be determined theoretically. Thus, N-O bond energies of 49.50, 48.62, and 48.07 kcal mol^{-1} could be calculated for **OXE-V**, **OXE-M**, and **OXE-P**, respectively. Significantly, energies of the triplet excited states of **OXE-M**, **OXE-V**, and **OXE-P** were theoretically calculated and indicated the triplet state to be higher than their N-O bond dissociation energies, so that photocleavage of oxime esters could occur from the triplet excited state. Cleavage enthalpies of **OXE-M**, **OXE-V**, and **OXE-P** were determined to be -4.03, 3.16, and -5.29 $kcal.mol^{-1}$, respectively. **OXE-M** was found to be able to outperform the final monomer conversion obtained with the reference compound diphenyl(2,4,6-trimethylbenzoyl)phosphine (TPO) (69% versus 65% for TPO) during the photopolymerization tests of TMPTA utilizing the different OXEs at 2×10^{-5} mol/g. This is directly related to the formation of methyl radicals by photocleavage and subsequent decarboxylation reaction. These radicals are carbon-centered radicals and methyl radicals are undoubtedly the most reactive ones. The best monomer conversions were attained with **OXE-M** for this reason. **OXE-P** and **OXE-V**, on the other hand, had lower monomer conversions (61 and 57%, respectively) due to the formation of less reactive radicals. Indeed, decarboxylation in this situation results in the production of aryl and vinyl radicals, which have lower reactivity than methyl radicals and support the lower monomer conversions reported with **OXE-P** and **OXE-V**. Finally, **OXE-H** (18%) had the lowest conversion, which is consistent with the fact that it is not an oxime ester and this molecule cannot, thus, cause any photocleavage (See Figure 11). The generation of methyl radicals, which are more reactive than aryl radicals (generated by photodecomposition of **OXE-P**) or vinyl radicals, is responsible of the higher monomer conversion attained with **OXE-M**. This reactivity trend is in line with results previously reported in the literature. [47]

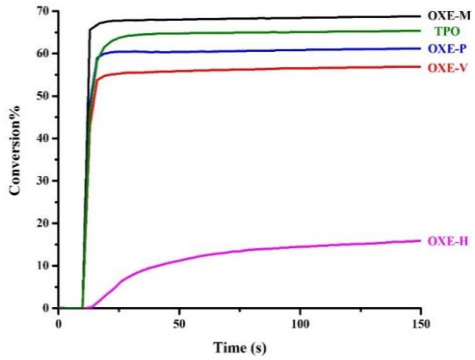

Figure 11. Photopolymerization profiles of TMPTA upon irradiation at 405 nm using OXE (2×10^{-5} mol/g). Reproduced with permission of Ref. [47].

Due to the strong reactivity of **OXE-M**, direct laser writing and 3D printing experiments were conducted with this oxime ester (See Figure 12). Patterns with a high spatial resolution could be found in both cases.

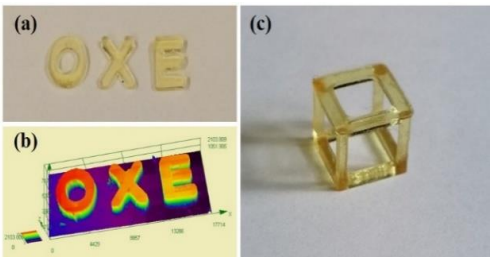

Figure 12. (a) The letter pattern "OXE" obtained by direct laser write; (b) Characterization of the letter pattern "OXE"; (c) 3D printed object of square frame (7×7×7 mm). Reproduced with permission of Ref. [47]

In this study, the dual photo/thermal initiation behaviors of **OXE-M**, **OXE-V** and **OXE-P** were also evidenced. DSC tests carried out in the dark revealed that **OXE-M** had the lowest onset temperature (113°C). Conversely, **OXE-V** and **OXE-P** showed higher initiation temperatures, above 150°C. The thermal initiation ability of **OXE-M** allowed the successful preparation of composites. TMPTA was combined with 50% carbon fiber to create prepregs, which were then heated at 150°C for 30 min to achieve a deep polymerization. The prepregs were then irradiated at 395 nm to polymerize the surface. Interestingly, fully cured carbon fiber-based composites could be obtained using this approach (See Figure 13).

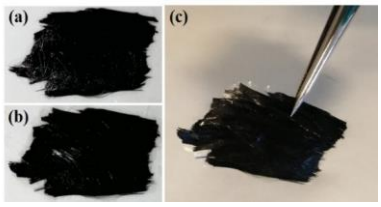

Figure 13. (a) Prepregs with resin/carbon fiber (50/50, wt%/wt%); (b) Surface cured prepregs; (c) Carbon fiber composite. Reproduced with permission of Ref. [47]

In 2022, our group evaluated 50 nitrocarbazole-based oxime esters, which were separated into five different series (See Figure 14). This study closely examined the influence of the oxime ester groups (acyloxy or aryloxy groups) on the photoinitiating ability but also the influence of the solubility of oxime esters in resins on the polymerization performance by adjusting the length of the carbazole chains or the length of the side chains. The use of nitrocarbazole as a common scaffold for the design of all of these dyes has been a crucial element in the development of this large series of oxime esters and to establish a structure/performance relationship. [48]

	Serie B	Serie C	Serie D	Serie E	Serie F
R=	B1	C1	D1	E1	F1
R=	B2	C2	D2	E2	F2
R=	B3	C3	D3	E3	F3
R=	B4	C4	D4	E4	F4
R=	B5	C5	D5	E5	F5
R=	B6	C6	D6	E6	F6
R=	B7	C7	D7	E7	F7
R=	B8	C8	D8	E8	F8
R=	B9	C9	D9	E9	F9
R= H	B10	C10	D10	E10	F10

Figure 14. Chemical structures of nitrocarbazole-based oxime esters. Reproduced with permission of Ref. [48]

It's interesting to note that the absorption maxima for all oxime esters stands between 370 and 372 nm (See Figure 15). Given that the molar extinction coefficients of all dyes are equivalent, influence of the solubility of oxime esters introduced by the functionalizing groups utilized to create oxime esters on the photoinitiating ability can thus be thoroughly investigated.

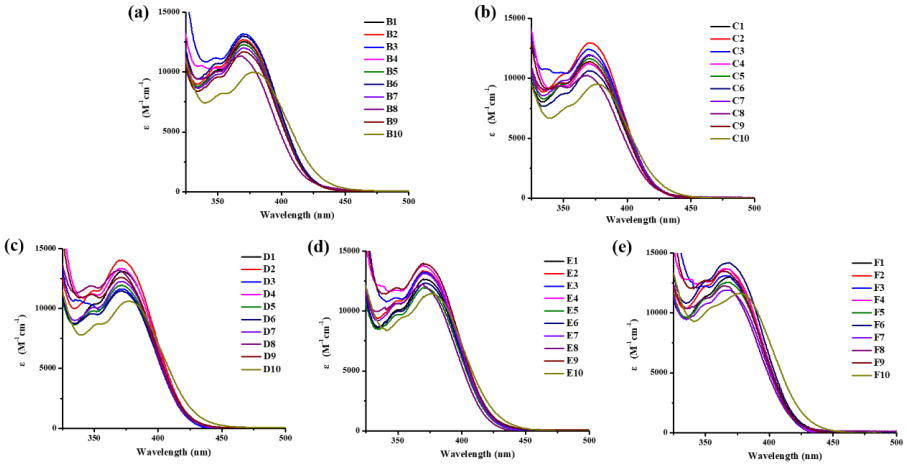

Figure 15. UV-visible absorption spectra of oxime esters in acetonitrile (a) OXEs based on Series B; (b) OXEs based on Series C; (c) OXEs based on Series D; (d) OXEs based on Series E; (e) OXEs based on Series F. Reproduced with permission of Ref. [48]

TMPTA was used as the monomer for the different polymerization experiments and the photoinitiating abilities of oxime esters **B1**–**B9**, **C1**–**C9**, **D1**–**D9**, **E1**–**E9**, and **F1**–**F9** were examined for TMPTA resins exposed to 405 nm light. According to Table 11, **OXEs 1** and **OXEs 2** containing acetyl or benzoyl groups continued to display the highest monomer conversions among the different series of oxime esters. **OXEs 8** bearing a nitrobenzoyl group, however, produced the worst monomer conversions. The reduced reactivity of the nitrobenzoyl radicals in this case was assigned to the electron-withdrawing ability of the nitro group, thereby deactivating the corresponding radicals. By comparing the different series of oxime esters, it is clear that the series D, which possesses a dodecyl chain on the carbazole unit and a butyryl group as the lateral chain could furnish the best monomer conversions. It can be thus concluded that the carbazole compounds with the most solubilizing chains can furnish the best monomer conversions. Only OXEs with an acetyl substituent (**B1**, **C1**, **D1**, **E1**, and **F1**) were able to

exceed the benchmark photoinitiator when their monomer conversions were compared to that obtained with TPO (66% conversion). Again, among the five series of oxime esters, **C1**, **D1**, and **F1** had the longest solubilizing chains. Other OXEs such as **D4** and **D5** showed remarkable performances compared to their analogues of the other series. Considering that all dyes have been designed to exhibit similar absorption properties, other parameters such as the decarboxylation reaction but also the reactivity of the generated radicals drastically impacted their photoinitiation abilities. Determination of the enthalpy for the decarboxylation reaction revealed the decarboxylation process to be only favorable for oxime esters bearing an acetyl group. For all the others, a less favorable decarboxylation process was evidenced, supporting the lower reactivity of the **B**/**C**/**D**/**E**/**F 2-9** series compared to the **B**/**C**/**D**/**E**/**F 1** series (See Table 12).

Table 11. The final function conversions (FCs) of TMPTA in the presence of OXEs.

PI	**B1**	**B2**	**B3**	**B4**	**B5**	**B6**	**B7**	**B8**	**B9**	**B10**
FC (%)	64	54	30	50	42	43	48	15	47	23
PIs	**C1**	**C2**	**C3**	**C4**	**C5**	**C6**	**C7**	**C8**	**C9**	**C10**
FC (%)	67	58	53	61	50	46	54	37	54	34
PI	**D1**	**D2**	**D3**	**D4**	**D5**	**D6**	**D7**	**D8**	**D9**	**D10**
FC (%)	68	62	56	61	59	58	58	41	55	35
PI	**E1**	**E2**	**E3**	**E4**	**E5**	**E6**	**E7**	**E8**	**E9**	**E10**
FC (%)	64	53	55	51	40	48	50	35	41	34
PI	**F1**	**F2**	**F3**	**F4**	**F5**	**F6**	**F7**	**F8**	**F9**	**F10**
FC (%)	68	56	54	58	45	51	53	36	57	38

Table 12. Enthalpies for the decarboxylation reactions for different acyloxy and aryloxy groups. Reproduced with permission of Ref. [48]

Decarboxylation reactions	$\Delta H_{decarboxylation}$ (kcal mol^{-1})
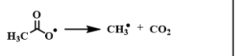	-4.94
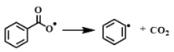	5.92
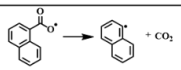	4.36
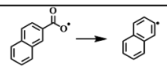	6.24
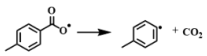	6.92
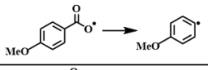	8.77
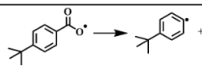	6.97
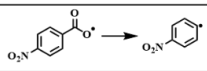	3.14
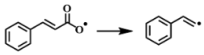	7.64

Analysis of their thermal initiating abilities revealed **B1** and **D1** to exhibit the lowest initial polymerization temperatures, according to the study done on the thermal initiating properties of **B1**, **C1**, **D1**, **E1**, and **F1**. For **B1** and **D1**, temperatures as low as 83 and 82°C were found respectively. Noticeably, the 50 oxime esters examined in this work showed this dual thermal/photochemical initiating behavior.

Still in 2022, a significant increase of the molar extinction coefficients could be obtained in the visible range by combining two carbazole units together. In this work, the 5,12-dihydroindolo[3,2-*a*]carbazole scaffold was used for elaborating a series of nine *bis*-oxime esters (see Figure 16).[49] Derivatives of *O*-acyloxy or *O*-benzoyloxy were therefore synthesized and developed. It should be noted that despite the fact that the 5,12-dialkyl-5,12-dihydroindolo[3,2-*a*]carbazole scaffold was originally described in 2019, only a small number of studies focused on its chemistry, particularly on asymmetrizing the substitution of this *bis*-carbazole structure. Since all oxime esters have comparable absorption characteristics, it was possible to precisely determine the reactivity of each group linked to the oxime function (See Figure 16). As a result of the polyaromatic structure of 5,12-dialkyl-5,12-dihydroindolo[3,2-

a]carbazole, absorption maxima at 379 nm for all dyes could be identified (See Figure 17). All dyes exhibited a tail extending in the visible range until ca. 410 nm except for **9** for which an absorption spectrum extending until 425 nm could be determined. In particular, the nitrobenzoyl derivatives (**dye 9**) showed the best absorption and outperformed the other dyes in terms of molar extinction coefficients (see Figure 17). Based on their absorptions, polymerization tests could be performed at 405 nm. An important issue in photopolymerization is the solubility of photoinitiators in resins as it can negatively impact the final monomer conversions. For this reason, a second series of compounds, called **2'-10'**, was prepared. These compounds **2'-10'** differ from the **2-10** series in that they have shorter alkyl chains (a methyl chain for **2'-10'** versus a hexyl chain for **2-10**). It has to be noticed that the absorption spectra of the **2-10** and **2'-10'** series were identical, enabling to compare their photoinitiating abilities with regards to their differences of solubility.

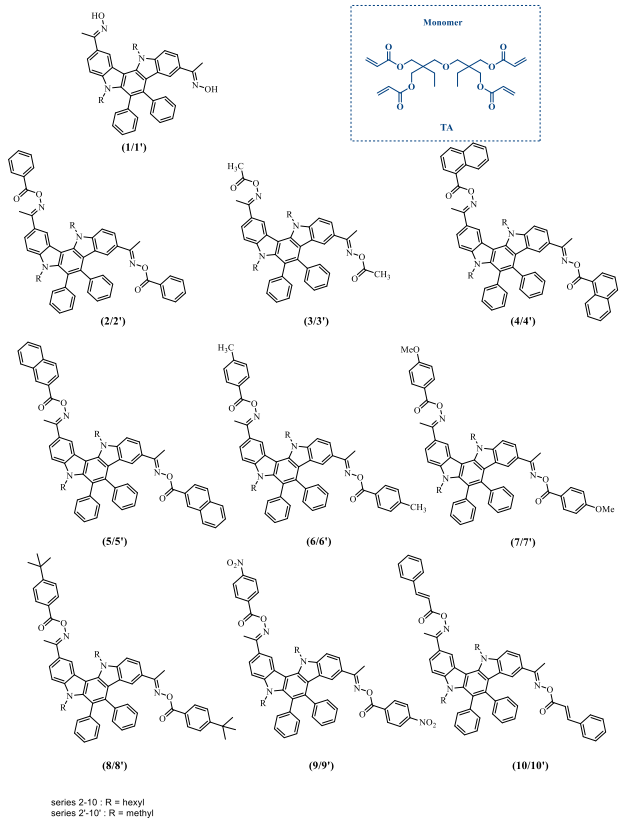

Figure 16. Chemical structures of 5,12-dialkyl-5,12-dihydroindolo[3,2-*a*]carbazole-derived oxime esters **2-10** and **2'-10'** and the monomer (TA). From ref. [49]

The higher reactivity of the methyl radicals over the others in thick and thin films was once again demonstrated during the polymerization tests performed in TMPTA after being exposed to a LED emitting at 405 nm. The TMPTA conversion could be improved by ca 20% using dye 3, as illustrated in Figure 18 and Table 13. The TMPTA conversions for **7**/**7'** and **9**/**9'**, which bear an electron-withdrawing or an electron-releasing group (OMe and NO_2 groups respectively) were the lowest. In the case of **9**/**9'**, low monomer conversions can be confidently assigned to the low solubility of the nitro derivatives in resins, even for compound **9** substituted with a hexyl chain.

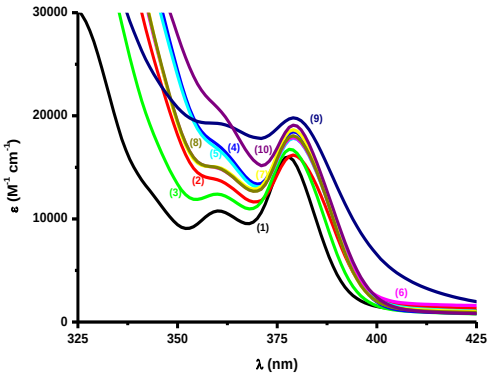

Figure 17. UV-visible absorption spectra of oxime esters **(1)-(10)** in toluene. Reproduced with permission of Ref. [49]

Again, proving that the reactivity is controlled by the solubility of oxime esters in resins, reduction of the solubilizing chain in **2'-10'** caused a significant decrease in the monomer conversion.

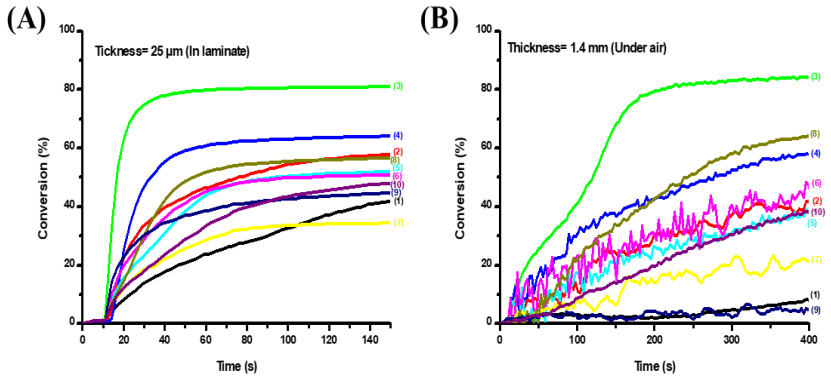

Figure 18. (A) Polymerization profiles of oxime esters **(1)-(10)** (0.5% w) in TMPTA in laminate (thickness = 25 µm) upon exposure to LED light λ = 405 nm using OXE (0.5% w). (B) Polymerization profiles of oxime esters **(1)-(10)** (0.5% w) in TMPTA under air (thickness = 1.4 mm) upon exposure to LED light λ = 405 nm using OXE (0.5% w). Reproduced with permission of Ref. [49]

Table 13. Final acrylate function conversions (FCs) and polymerization rates for TMPTA using one component (0.5% w) photoinitiators after irradiation with LED light (λ= 405 nm).

OXE	Thin sample (25 µm) in laminate	OXE	Thin sample (25 µm) in laminate	OXE	Thick sample (1.4 mm) under air	OXE	Thick sample (1.4 mm) under air
(1)	42%	**(1')**	29%	**(1)**	8%	**(1')**	15%
(2)	58%	**(2')**	38%	**(2)**	50%	**(2')**	61%
(3)	81%	**(3')**	82%	**(3)**	84%	**(3')**	81%
(4)	64%	**(4')**	66%	**(4)**	58%	**(4')**	38%
(5)	52%	**(5')**	49%	**(5)**	39%	**(5')**	34%
(6)	51%	**(6')**	41%	**(6)**	45%	**(6')**	58%
(7)	35%	**(7')**	47%	**(7)**	21%	**(7')**	35%
(8)	57%	**(8')**	54%	**(8)**	65%	**(8')**	54%
(9)	45%	**(9')**	28%	**(9)**	5%	**(9')**	19%
(10)	48%	**(10')**	49%	**(10)**	39%	**(10')**	41%

The bond dissociation energy for the N-O bonds in all oxime esters was calculated to be between 41 and 43 kcal/mol. For this series of carbazole, photocleavage was also found to occur from the singlet excited state, since the process was unfavorable from the triplet excited state, according to the determination of the enthalpy of cleavage (See Table 14).

Table 14. Parameters characterizing the investigated OXEs **(1)-(10)**. Some parameters were calculated by molecular modelling: the bond dissociation energy BDE (N-O), the triplet state energy E_{T1} and the enthalpy $\Delta H_{cleavage\ T1}$ for the cleavage from T_1. The singlet excited state energy E_{S1}, the enthalpy $\Delta H_{cleavage\ S1}$ for the cleavage from S_1, and the fluorescence lifetime of the OXEs were measured experimentally.

OXE	BDE (N-O) (kcal.mol^{-1})	E_{S1} (kcal mol^{-1})	$\Delta H_{cleavage\ S1}$ (kcal mol^{-1})	E_{T1} (kcal mol^{-1})	$\Delta H_{cleavage\ T1}$ (kcal mol^{-1})
(1)	-	74.25	-	62.21	-
(2)	41.55	73.1	-31.55	62.22	-20.67
(3)	47.02	73.56	-26.54	52.15	-5.13
(4)	40.56	72.87	-32.31	58.09	-17.53
(5)	41.35	73.33	-31.98	52.14	-10.79
(6)	41.28	73.33	-32.05	62.16	-20.88

(7)	40.88	73.33	-32.45	62.15	-21.27
(8)	41.25	73.1	-31.85	62.20	-20.95
(9)	43.71	-	-	62.07	-18.36
(10)	42.97	66.88	-23.91	52.45	-9.48

Interestingly, it could be established in these different works how much more reactive were the aliphatic radicals compared to the aryl radicals. The solubility issue has negatively impacted the photoinitiating ability of numerous dyes, even though numerous high-performance photoinitiating systems could be developed with these scaffolds. Up to now, most of the oxime esters reported in this review exhibited an absorbance standing in the 450–500 nm range. Future work will consist in creating oxime esters with absorptions more redshifted than those now attained in order to achieve an enhanced light penetration within the photocurable resins. Future research will also focus on creating oxime esters with this dual capability for triggering thermal and photochemical reactions.

5. Polyaromatic oxime esters: Naphthalene, Pyrene and Anthracene chromophores

Naphthalene and its derivatives, polyaromatic hydrocarbons based on fused aromatic rings have also been developed to act as Type I photoinitiators. It is anticipated that a naphthalene-based photoinitiator, due to the remarkable planarity of naphthalene will favor the electron delocalization. Polyaromaticity is also favorable for the preparation of dyes with high molar extinction coefficients. Recently, a series of naphthalene-based oxime esters was elegantly proposed, these structures exhibiting a significant absorption for $\lambda < 400$ nm. [50] In order to get a bathochromic shift of the absorption maxima, other polyaromatic structures were proposed. The family of Polycyclic Aromatic Hydrocarbons (PAHs), which includes pyrene, a polyaromatic structure made up of four fused aromatic rings, is the focus of interdisciplinary research in the domains of chemistry, physics, materials science, and biology. More particular, pyrene has undergone substantial research for the development of photoluminescent materials. In the solid form, pyrene has a photoluminescence quantum yield of 0.68. However, pyrene has a strong tendency to dimerize at high concentrations, which has a negative impact on its solubility in the majority of common organic compounds, as frequently found for planar polyaromatic structures. [51-53] Many empirical and semi-empirical models have been proposed in the literature to explain this phenomenon. [54] At the same time, the fluorescence of pyrene frequently coexists with that of excimers due to pyrene dimerization. *Tert*-butyl groups are often

added to the 2,7-positions of pyrene to address the solubility issue, but since this chemical is still quite expensive, research is still ongoing to find a simple substitution technique for pyrene. Pyrene remains a useful building block for the preparation of photoinitiators due to its long excited state lifetime (50-90 ns), ease of functionalization by simple reactions such as bromination, Vilsmeier-Haak or Friedel-Crafts acylation processes, and many other standard reactions. Photophysical properties of pyrenes have been thoroughly studied and documented in the literature, making them a reliable basis for the development of visible light photoinitiators. In addition, anthracene has been found to be a promising scaffold in the search for new Type I structures, as it works well as a UV photoinitiator. [55-57] Anthracene is a polyaromatic structure frequently used in Organic Electronics to create fluorescent probes, singlet emitters for organic light-emitting diodes, and dyes for solar cells. The low oxidation potential of this structure, its good film-forming ability make it an excellent candidate for elaborating multilayered devices. [58-61] However, photopolymerization is also part of the range of applications of anthracene. Recently, our group have used an innovative approach to develop novel type I photoinitiators through a combination of these two chromophores i.e. pyrene and anthracene that could act as Type I photoinitiators when linked to an oxime ester group. [62] Two series of oxime esters were prepared (See Figures 19 and 20). The anthracene chromophore (An-OXE) is present in the first family composed of 17 compounds, and the pyrene moiety is present in the second family composed of 18 compounds (Py-OXE). The two structures, namely pyrene and anthracene, were selected for this study as pyrene and anthracene respectively react from their first excited singlet (S1) and triplet (T1) states. Therefore, impact of the chromophore (pyrene vs. anthracene) on their photochemical characteristics and photoinitiating abilities could be investigated in this work. The newly proposed PIs (An-OXEs and Py-OXEs) were characterized by good near-UV and visible absorption properties.

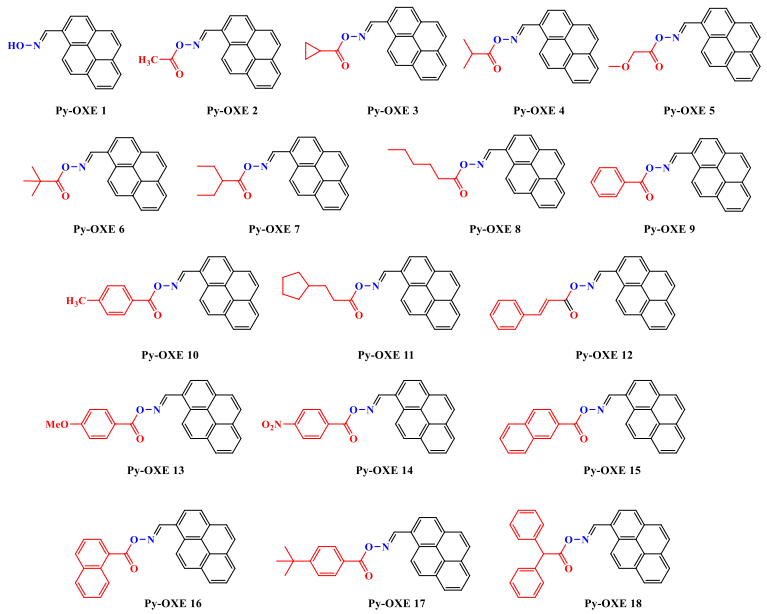

Figure 19. Chemical structures of the Py-OXE series investigated. Reproduced with the permission from [62].

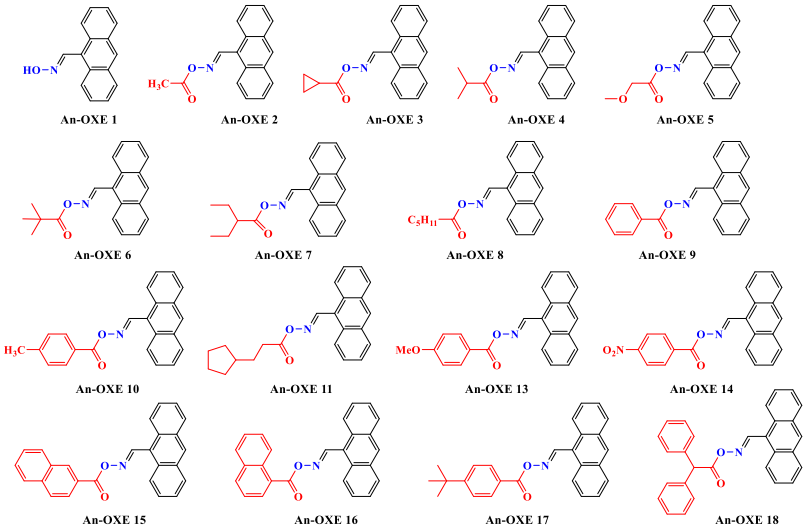

Figure 20. Chemical structures of the An-OXE series examined. Reproduced with the permission from [62].

Starting with the readily available 9-anthracenecarboxaldehyde or 1-pyrenecarboxaldehyde, all oxime esters examined in this work were produced in two steps. The two oximes could be prepared in the first step by reacting the appropriate aldehyde with hydroxylamine hydrochloride under basic conditions. Specifically, sodium acetate, a water-soluble base, was chosen. Methanol, THF, and water were used as a mixture of three solvents to carry out the reaction. Reaction yields greater than 96% enabled the production of the two oximes. Surprisingly, when oxime esterification was studied, the anthracene-9-carbaldehyde oxime (**An-OXE 1**) failed to form esters if triethylamine was used as a base. Instead, a dehydration reaction was observed, producing the unusual reaction product anthracene-9-carbonitrile. By slowly evaporating chloroform, crystals of this compound could be obtained, allowing X-ray diffraction to clearly identify the substance's chemical structure. Surprisingly, the different oxime esters could be prepared without using base. Thus, anthracene-9-carbaldehyde oxime was combined with one equivalent of the appropriate acid chloride and could produce the different anthracene-based oxime esters in high yields. The various esters were prepared using 17 distinct acid chlorides, ranging from aromatic to aliphatic acid chlorides (See Scheme 6). The possibility of generating aromatic but also aliphatic primary, secondary,

and tertiary radicals, stabilized and destabilized radicals during the cleavage and decarboxylation reaction of radicals served as a notable justification for the diversity of acid chlorides. Only the cinnamoyl derivative, or **An-OXE 12**, could not be obtained in the case of the anthracene-based oxime esters, despite numerous attempts. For the pyrene-based oxime esters, the different compounds **Py-OXE 2**-**Py-OXE 18** could be prepared under standard conditions by deprotonation of pyrene-1-carbaldehyde oxime (**Py-OXE 1**) with an excess of triethylamine and by esterification with the proper acid chlorides. Table 15 provides a summary of the reaction yields.

Table 15. Reaction yields obtained during the esterification of the two oximes.

esters	**Py-OXE 1**	**Py-OXE 2**	**Py-OXE 3**	**Py-OXE 4**	**Py-OXE 5**	**Py-OXE 6**	**Py-OXE 7**	**Py-OXE 8**	**Py-OXE 9**
reaction yields (%)	96	86	81	84	83	80	94	91	80
esters	**Py-OXE 10**	**Py-OXE 11**	**Py-OXE 12**	**Py-OXE 13**	**Py-OXE 14**	**Py-OXE 15**	**Py-OXE 16**	**Py-OXE 17**	**Py-OXE 18**
reaction yields (%)	80	83	68	87	93	86	81	83	85
esters	**An-OXE 1**	**An - OXE 2**	**An - OXE 3**	**An - OXE 4**	**An - OXE 5**	**An - OXE 6**	**An - OXE 7**	**An - OXE 8**	**An - OXE 9**
reaction yields (%)	98	78	89	88	82	76	77	88	82
esters	**An - OXE 10**	**An - OXE 11**	**An - OXE 12**	**An - OXE 13**	**An - OXE 14**	**An - OXE 15**	**An - OXE 16**	**An - OXE 17**	**An - OXE 18**
reaction yields (%)	88	84	n.o.[1]	72	86	74	78	88	92

[1] : not obtained.

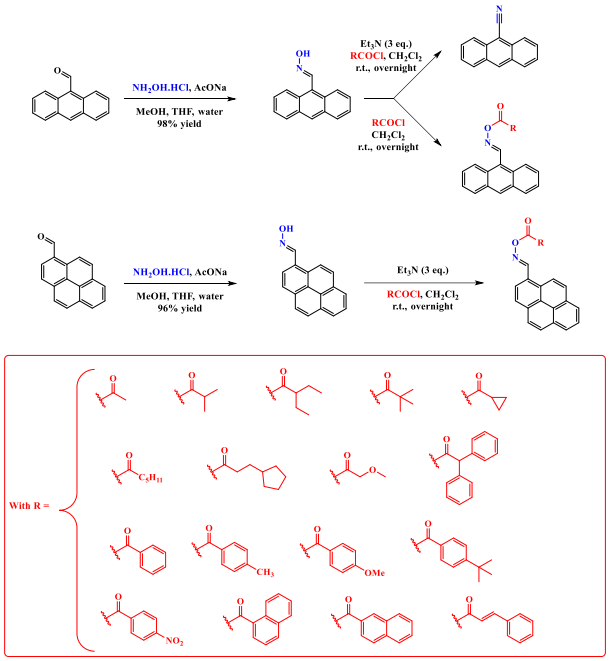

Scheme 6. Synthetic routes to the different anthracene and pyrene-based oxime esters.

Figure 21 presents the UV-visible absorption spectra of the different pyrene-based OXEs in acetonitrile (ACN) (See also Table 16). Following is a comparison with the different absorptions of An-OXEs. For example, $\varepsilon_{Py\text{-}OXE}$ = 52 000 $M^{-1}{\cdot}cm^{-1}$ at 361 nm for **Py-OXE2**; 42 500 $M^{-1}{\cdot}cm^{-1}$ at 362 nm for **Py-OXE3**; and 40 600 $M^{-1}{\cdot}cm^{-1}$ at 364 nm for **Py-OXE12** are examples of organic compounds with a broad absorption band and a strong ability to absorb light in the near-UV and visible range between 300-425 nm. Indeed, these oxime esters exhibit good absorption properties at 405 nm, ensuring a good overlap with the emission spectra of the LEDs utilized in this work (λ_{exc} = 405 nm).

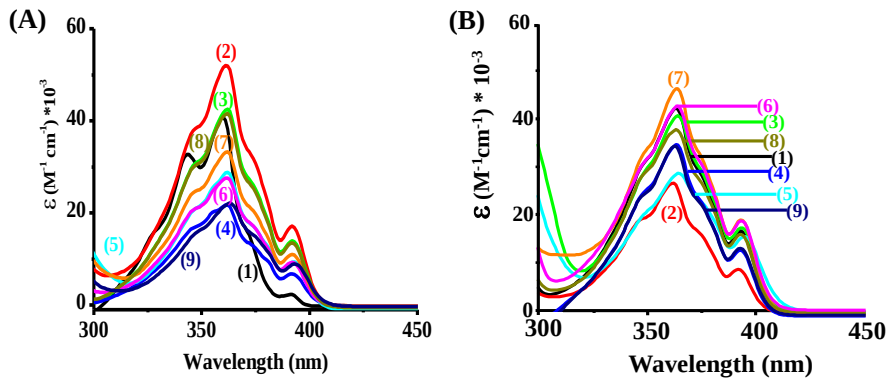

Figure 21. UV-visible absorption spectra of the Py-OXE derivatives in ACN: (1) **Py-OXE 1**, (2) **Py-OXE 2**, (3) **Py-OXE 3**, (4) **Py-OXE 4**, (5) **Py-OXE 5**, (6) **Py-OXE 6**, (7) **Py-OXE 7**, (8) **Py-OXE 8**, (9) **Py-OXE 9**. (B) UV-visible absorption spectra of the Py-OXE derivatives in ACN: (1) **Py-OXE 10**, (2) **Py-OXE 11**, (3) **Py-OXE 12**, (4) **Py-OXE 13**, (5) **Py-OXE 14**, (6) **Py-OXE 15**, (7) **Py-OXE 16**, (8) **Py-OXE 17**, (9) **Py-OXE 18**. Reproduced with permission of Ref.[61].

Table 16. Absorption properties of Py-OXEs at λ_{max} and 405 nm in acetonitrile (ACN).

	λ_{max} (nm)	ε_{max} (M^{-1} cm^{-1})	ε_{405nm} (M^{-1} cm^{-1})
Py-OXE1	359	40500	0
Py-OXE2	361	52000	1340
Py-OXE3	362	42500	1160
Py-OXE4	361	21760	580
Py-OXE5	362	28830	535
Py-OXE6	362	27560	770
Py-OXE7	362	33300	1100
Py-OXE8	362	41560	960
Py-OXE9	362	22000	1530
Py-OXE10	362	42190	2620
Py-OXE11	362	26570	545
Py-OXE12	364	40600	4110
Py-OXE13	363	34630	1200
Py-OXE14	362	28640	6400
Py-OXE15	364	42600	4400
Py-OXE16	364	46300	3400
Py-OXE17	363	37720	2720
Py-OXE18	362	34250	1560

TA was used as a benchmark monomer for FRP tests in thin samples employing An-OXEs as Type I photoinitiators (0.5% w/w). Figure 22 depicts the various FRP profiles (conversion vs. irradiation time), and Table 17 provides an overview of the conversion data. First of all, the different oxime esters based on anthracene exhibited moderate polymerization efficiencies, leading the majority of An-OXEs to furnish low final acrylate function conversions (FCs) when exposed to an irradiation at 405 nm. For example, for **An-OXE2** FC = 32%, for **An-OXE4 FC =** 50%, and for **An-OXE6**, FC = 34%. No polymerization occurred for TA (without PIs), indicating the crucial role of An-OXEs in the monomer conversion.

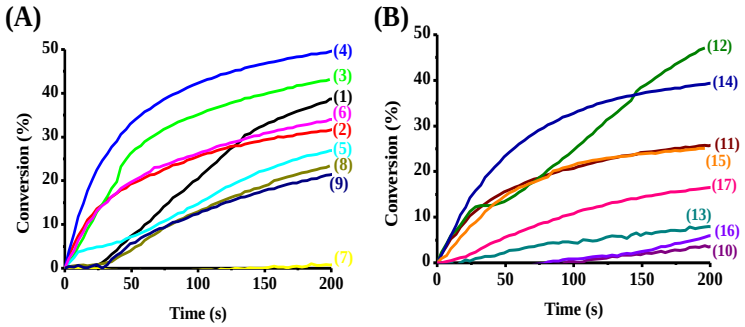

Figure 22. (A), (B) Photopolymerization profiles of acrylates functions using the TA monomer (acrylate function vs. irradiation time) performed in Thin sample in laminate upon irradiation at 405 nm using one-component PISs (0.5%): **(1) An-OXE 1**, **(2) An-OXE 2**, **(3) An-OXE** 3, **(4) An-OXE 4**, **(5) An-OXE 5**, **(6**) **An-OXE 6**, **(7) An-OXE 7**, **(8) An-OXE 8**, **(9) An-OXE 9**, **(10) An-OXE 10**, **(11) An-OXE 11, (12) An-OXE 13, (13) An-OXE 14, (14) An-OXE 15, (15) An-OXE 16 (16) An-OXE 17, (17) An-OXE 18**. Irradiation starts at t = 0 s. Reproduced with permission of Ref.[61]

When a pyrene group was used instead of the anthracene chromophore (Py-OXE), a different trend was found. Here again, polymerization tests were carried out in laminate, in thin films upon irradiation at 405 nm (I = 110 mW/cm^2) with a LED. Figure 23 displays the photopolymerization profiles, and Table 17 contains the results obtained during the FRP of TA in laminate. When comparing the monomer conversions obtained during the FRP of TA by the different Py-OXE (0.5% w) systems to those obtained with the An-OXE analogues, for instance, monomer conversions of 79% for **Py-OXE2**; 63% for **Py-OXE3**; 74% for **Py-OXE4**; and 76% for **Py-OXE 7** were obtained, greatly higher than that obtained for the An-OXE analogues. Thus, conversions of 32% for **An-OXE2**; 43% for **An-OXE3**; and 50% for **An-OXE4** were determined after 200 s of irradiation. Working with pyrene derivatives resulted in significantly increased polymerization. In contrast to the oxime esters, which contain an anthracene chromophore that has limited photoinitiation capacity, these data clearly

demonstrate the substantial impact of pyrene on the polymerization profiles of acrylate functionalities. The findings also demonstrated that Py-OXE with alkyl substituents on the ester moieties have greater polymerization efficiency, as demonstrated by FC = 79% for **Py-OXE2** with methyl group against 25% for **Py-OXE15** with a naphthyl group.

It is important to note that these oxime esters showed great efficiency compared to the reference structures (**Py-OXE1** or **An-OXE1**) which possess a N-OH group unable to fragment and generate radicals. This clearly shows the interest of the oxime ester functions in the photopolymerization process e.g. FC = 14% for **Py-OXE1** vs. 79% **Py-OXE2**.

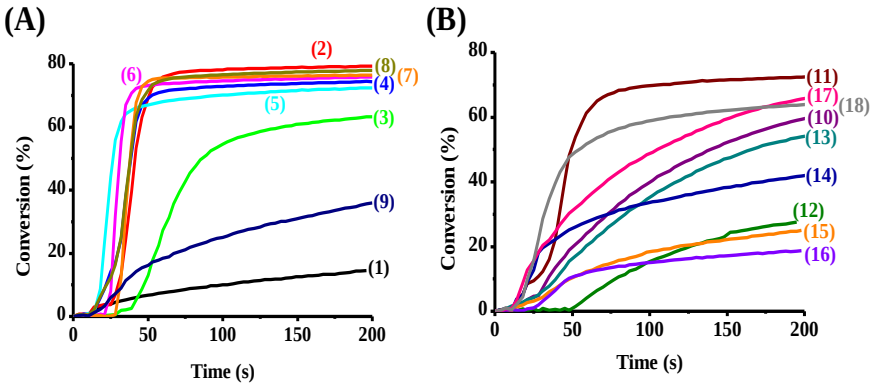

Figure 23. (A), (B) Photopolymerization profiles of acrylates functions using the TA monomer (acrylate function vs. irradiation time) performed in Thin sample in laminate upon irradiation at 405 nm using one-component PISs (0.5%): **(1) Py-OXE 1**, **(2) Py-OXE 2**, **(3) Py-OXE 3**, **(4) Py-OXE 4**, **(5) Py-OXE 5**, **(6) Py-OXE 6**, **(7) Py-OXE 7**, **(8) Py-OXE 8, (9) Py-OXE 9, (10) Py-OXE 10, (11) Py-OXE 11**, **(12) Py-OXE 12**, **(13) Py-OXE 13**, **(14) Py-OXE 14**, **(15) Py-OXE 15 (16) Py-OXE 16**, **(17) Py-OXE 17**, **(18) Py-OXE 18**. Irradiation starts at t = 15 s. Reproduced with permission of Ref.[61]

Table 17. Final reactive (acrylate) function conversions (FC%) for TA using Py-OXEs or An-OXEs upon visible light irradiation using the LED @405 nm in laminate.

	Py-OXE	**An-OXE**
OXE-1	14%	39%
OXE-2	79%	32%
OXE-3	63%	43%
OXE-4	74%	50%
OXE-5	72%	27%
OXE-6	76%	34%

OXE-7	76%	23%
OXE-8	78%	0%
OXE-9	36%	22%
OXE-10	60%	0%
OXE-11	72%	26%
OXE-12	28%	-
OXE-13	54%	47%
OXE-14	42%	0%
OXE-15	25%	39%
OXE-16	19%	25%
OXE-17	66%	0%
OXE-18	64%	16%

These results can be explained in terms of bond dissociation energy. Indeed, for **Py-OXE1**, the bond dissociation energy of the N-O bond is higher than that determined for the different oxime esters. Thus, a BDE N-O = 61.15 kcal/mol could be determined for **Py-OXE1** vs. 47.86, 45.65, 47.39, and 47.82 kcal/mol for **Py-OXE2**,**3**,**4**,**5**, respectively (See Table 18), accompanied by an elongated excited state lifetime for **Py-OXE1** compared to Py-OXEs, which strongly suggests a singlet state cleavage process (τ_0 = 6.8 ns for **Py-OXE1** vs. 3.8, 3.66, 3.8, 3.14 ns for **Py-OXE2,3,4,5**) (See Table 18). Cleavage from the singlet excited state S_1 is shown to be more favorable (ES1 > BDE (N-O)), whereas cleavage from the triplet excited state is less favorable (E_{T1} BDE (N-O)), as shown for example for **Py-OXE2** (E_{S1} = 71.72 kcal/mol; E_{T1} = 41.56 kcal/mol vs. BDE (N-O) = 47.86 kcal/mol.

Table 18. Parameters characterizing the An-OXEs and Py-OXEs. Some parameters characterizing the proposed PIs were calculated by molecular modelling: the bond dissociation energy BDE (N–O), the triplet state energy E_{T1}, the singlet excited state energy E_{S1} (evaluated experimentally from the experimental absorption and fluorescence spectra). The S_1 excited state lifetimes were determined by time resolved fluorescence spectroscopy.

PI	**BDE_{N-O} (kcal/mol)**	**E_{S1} (kcal/mol)**	**τ_0 (S_1) (ns)**	**E_{T1} (kcal/mol)**
1	63.25[a] 61.15[b]	68.95[a] 74.49[b]	4.58[a] 6.8[b]	33.75[a] 41.70[b]
2	44.95[a] 47.86[b]	66.41[a] 71.72[b]	1.5[a] 3.8[b]	39.54[a] 41.56[b]

3	45.74 [a] 45.65 [b]	n.d	3.66 [b]	34.48 [a] 41.48 [b]
4	44.73 [a] 47.39 [b]	n.d	3.8 [b]	34.08 [a] 41.56 [b]
5	46.98 [a] 47.82 [b]	n.d	3.14 [b]	34.34 [a] 41.39 [b]
6	43.78 [a] 46.70 [b]	n.d	3.75 [b]	39.72 [a] 41.53 [b]
7	43.72 [a] 46.84 [b]	n.d	3.7 [b]	39.55 [a] 41.55 [b]
8	46.33 [a] 46.66 [b]	n.d	3.79 [b]	34.28 [a] 41.40 [b]
9	44.48 [a] 47.34 [b]	n.d	3.02 [b]	39.48 [a] 41.43 [b]
10	46.60 [a] 47.17 [b]	n.d	2.56 [b]	34.47 [a] 41.43 [b]
11	44.92 [a] 47.94 [b]	n.d	2.57 [b]	39.48 [a] 41.57 [b]
12	43.65 [b]	n.d	n.d	43.45 [b]
13	46.29 [a] 46.93 [b]	n.d	n.d	34.46 [a] 41.43 [b]
14	46.52 [a] 45.00 [b]	n.d	n.d	39.37 [a] 43.57 [b]
15	44.34 [a] 42.92 [b]	n.d	n.d	39.47 [a] 43.65 [b]
16	45.59 [a] 41.88 [b]	n.d	n.d	34.65 [a] 43.50 [b]
17	46.61 [a] 47.17 [b]	n.d	n.d	34.50 [a] 41.43 [b]
18	44.61 [a] 47.65 [b]	n.d	n.d	33.80 [a] 41.56 [b]

a: An-OXE
b: Py-OXE
n.d: not determined

Figures 23 and 24 and Table 17 compare how the anthracene and the pyrene chromophores affect the absorption characteristics of the corresponding oxime esters and therefore the photoinitiating ability. The results obtained showed that the oxime esters comprising the pyrene chromophore had a higher initiation ability than those prepared with anthracene. For example, is the final conversion 32% for **An-OXE2** and 79% for **Py-OXE 2**, Table 17. Pyrene derivatives are more reactive which is in agreement with their higher cleavage capacity, despite the fact that anthracene-based oxime esters absorb more light at 405 nm than pyrene oxime esters ($\varepsilon = 4000$ vs. 1580 $M^{-1}cm^{-1}$ for **An-OXE 2** and **Py-OXE 2**, respectively) (see Figure 24). Overall, from these comparisons, it can be concluded that photocleavage of these oxime esters is more favorable from the singlet excited state than the triplet state, the fast

photocleavage of oxime esters improving the monomer conversion by limiting radicals recombination.

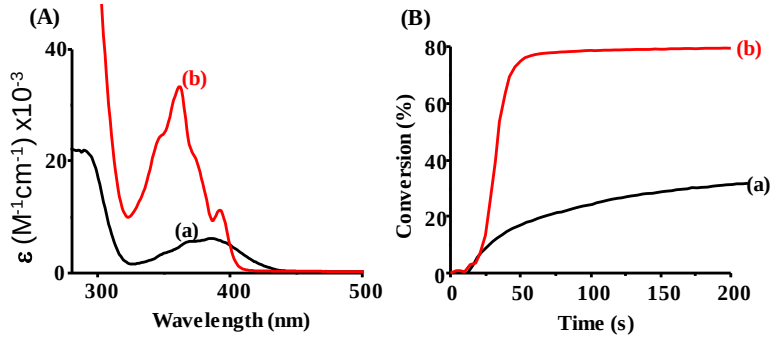

Figure 24. (A) UV-visible absorption spectra of **(a)** An-OXE 2 and **(b)** Py-OXE 2. **(B)** Photopolymerization profiles of acrylates functions using **(a)** An-OXE 2 (0.5% w) and **(b)** Py-OXE 2 (0.5% w) as photoinitiators. Reproduced with permission of Ref. [61]

The different results revealed that the newly proposed oxime esters, particularly those based on pyrene had extremely good photoinitiating abilities competing with other families such as coumarins or carbazoles. This discovery paves the way for the development of brand-new Type I photoinitiators based on pyrene that exhibits a more redshifted absorption towards the visible range.

6. Phenothiazine based-oxime esters

Phenothiazine (PTZ) is an inexpensive compound that is simple to modify. Due to the inclusion of this molecule in numerous drugs, its chemistry was extensively studied in the 1970s so that photopolymerists could benefit from these advances in phenothiazine chemistry. [63-65] In-depth research on phenothiazine was also done to develop chromophores specifically designed for dye-sensitized solar cells. In relation to photopolymerization, Margerum and coworkers published in 1969 the first study indicating the use of phenothiazines as photoinitiators of polymerization. In this groundbreaking study, phenothiazine was used as a photooxidant capable to oxidize methylene blue or thionine in the excited state, thus producing initiating radicals for the FRP of barium diacrylate. Following this research, phenothiazine was frequently used as a UV photoinitiator for photoinduced charge transfer polymerization of acrylonitrile through the formation of an exciplex between phenothiazine and acrylonitrile, the polymerization of tetrahydrofuran using triphenylsulfonium hexafluoroarsenate, and upon sensitization of the reaction by phenothiazine. More recently, various two-component

phenothiazine/sulfonium salt initiating systems have been employed as photochemical initiators for the CP of epoxides and the FRP of acrylates. [65-67]

A series of oxime esters based on phenothiazine were recently synthesized and proposed as high-performance photoinitiating systems (Scheme 7) (Unpublished results from IS2M). Photoreactivity of the studied compounds was evaluated after exposure of the resins to LEDs emitting at 405 nm.

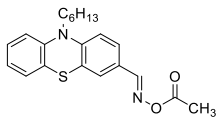

PTZ

Scheme 7. Chemical structure and abbreviation of the synthesized phenothiazine-based OXE.

PTZ has a high molar extinction coefficient (about 7000 $M^{-1}.cm^{-1}$), as shown in Figure 25. As a result, the absorption characteristics of the investigated oxime ester enabled a good overlap with the emission spectra of the visible LED used in this work.

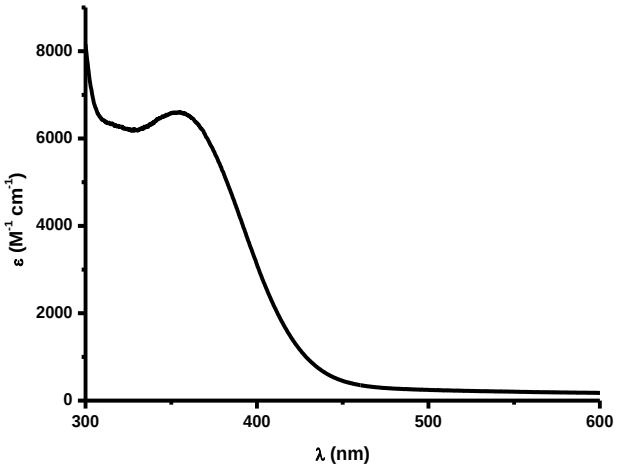

Figure 25. UV-visible absorption properties of **PTZ** in acetonitrile. Unpublished results @IS2M.

Photopolymerization experiments done under LED@ 405 nm revealed the good reactivity of PTZ. Moreover, **PTZ** showed a reactivity very close to that of the commercial photoinitiator TPO (see Figure 26).

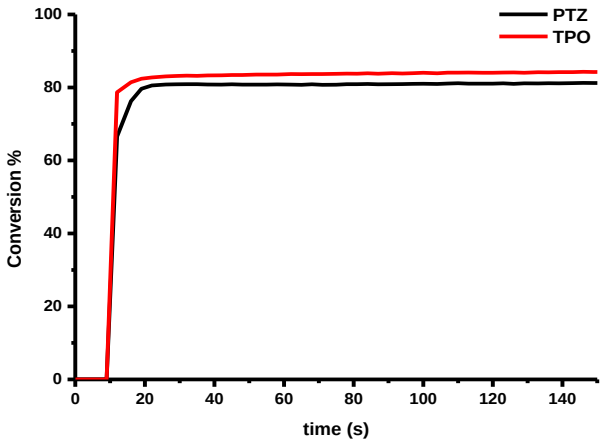

Figure 26. Photopolymerization profiles of TA (acrylate function conversion vs. irradiation time) in laminate (thickness = 25 µm) upon exposure to a LED (λ = 405 nm) in the presence of PIs (1%w/w). The irradiation starts at t = 10 s. Unpublished results @IS2M.

7. Oxime esters analogues

7.1. Naphthoquinone-based imidazolyl esters

Functional metabolites based on naphthoquinone derivatives (NQs) can be found in nature in a variety of sources, including plants, bacteria, and marine species. They are readily available and easy to obtain without complex synthetic procedures and these compounds are also well-known to exhibit anticancer properties. [69] Additionally, the naphthoquinone structure can have various functional groups added on it, enabling to drastically modify the light absorption and notably to redshift their absorptions towards longer wavelengths. Noticeably, naphthoquinones have never been investigated as Type I photoinitiators before 2022. [70] Therefore, investigation of naphthoquinone for the design of photoinitiating systems and examination of the impact of the structural variations on their photoinitiating abilities is therefore exciting and important. Recently, a study conducted by Lalevée and coworkers investigated and proposed an unprecedented class of naphthoquinone esters — the 4,9-dioxo-2-phenyl-4,9-dihydro-1*H*-naphtho[2,3-*d*]imidazol-1-yl esters — as high-performance Type I PIs (See Scheme 8). [71] In

order to prepare this series of imidazolyl esters easily, different acid chlorides were used to generate the different esters with 1-hydroxy-2-phenyl-1*H*-naphtho[2,3-*d*]imidazole-4,9-dione. This family of imidazolyl esters, which is novel in the literature and whose structure is comparable to that of the well-known family of oxime esters, is also capable to initiate an homolytic cleavage of the N-O bond upon irradiation. Decarboxylation may also occur after cleavage, generating initiating aryl or alkyl radicals. Considering the similarity of structures between imidazolyl esters and oxime esters, investigation of this new class of PIs and the determination if this family of imidazolyl esters could act as high-performance PIs in comparison to oxime esters or the well-known phosphine oxides was of crucial importance for us (e.g. TPO; Scheme 3). Their abilities to initiate a photopolymerization process under mild conditions (low light intensity using LEDs emitting at 405 nm or 455 nm) was studied. Another indication of their high reactivity is the possibility of using them in photosensitive 3D printing resins.

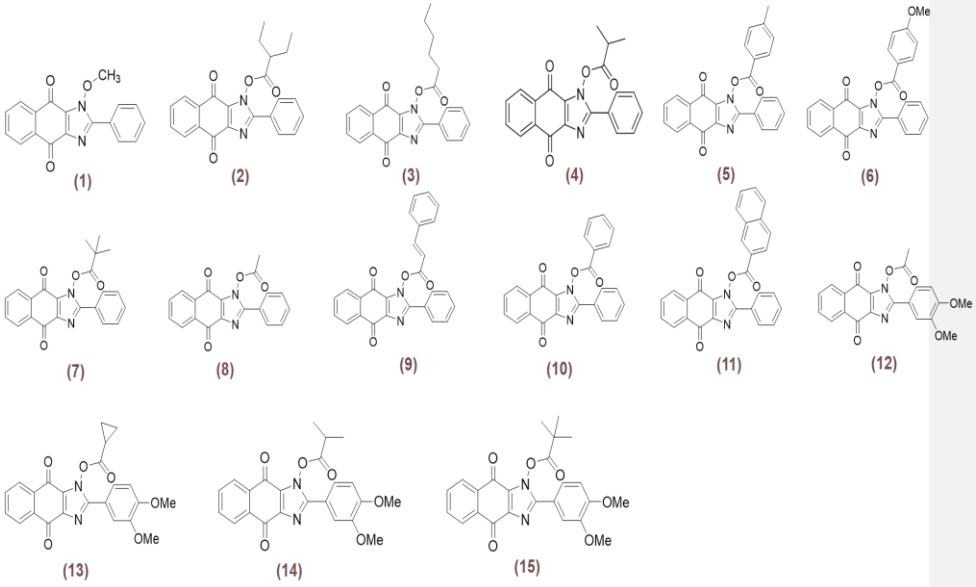

Scheme 8. Chemical structures of the synthesized naphthoquinone-based imidazolyl esters. Reproduced with the permission from Ref. [72].

Concerning the synthesis of these imidazolyl esters, 1,4-naphthoquinone (C1) was used as the starting material to prepare all dyes (See Scheme 9). 2-(Benzylamino)naphthalene-1,4-dione (C4) and 2-((3,4-dimethoxylbenzyl)amino)naphthalene-1,4-dione (C5) were obtained in

92 and 85% yields, respectively, by a Michael condensation of benzylamine (C2) and 3,4-dimethoxybenzylamine (C3). Compounds 1-hydroxy-2-phenyl-1*H*-naphtho[2,3-*d*]imidazole-4,9-dione (C6) and 2-(3,4-dimethoxyphenyl)-1-hydroxy-1*H*-naphtho[2,3-*d*]imidazole-4,9-dione (C7) could be produced in 67 and 84% yields, respectively, by a cyclization procedure previously reported by Lavrikova and coworkers. Precisely, derivatives of 1-hydroxy-2-phenyl-1*H*-naphtho[2,3-*d*]imidazole-4,9-dione C6 and C7 were esterified using triethylamine as the base and the appropriate acid chlorides so that compounds 2-15 could be obtained. This method therefore produced compounds that can be regarded as oxime ester analogues. A molecule with a non-cleavable group was also prepared for comparison. Thus, 1-methoxy-2-phenyl-1*H*-naphtho[2,3-*d*]imidazole-4,9-dione (1) could be obtained in pure form in 88% yield after alkylation of C6 with iodomethane in DMF at room temperature and utilizing potassium *tert*-butoxide as the base.

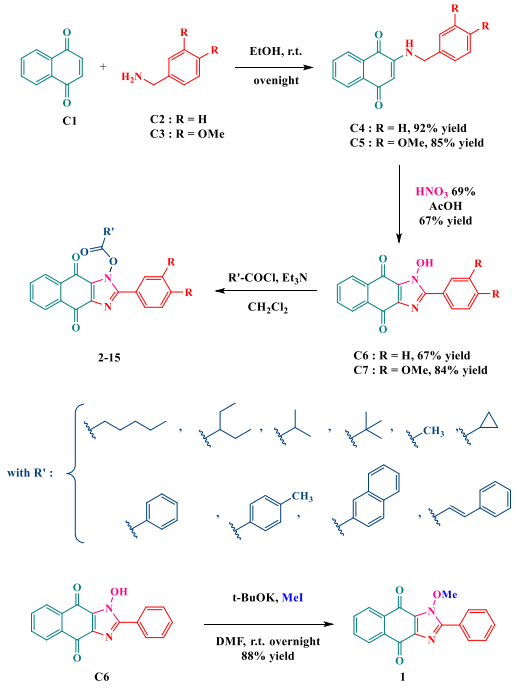

Scheme 9. Synthetic routes to the different dyes. Reproduced with the permission from Ref. [72].

Acetonitrile (ACN) was used as the solvent to acquire the UV-visible absorption spectra of the investigated derivatives (See Figure 27), and Table 19 lists the main parameters.

Compounds **(1)-(11)** exhibited a maximum absorption at about 380 nm, but the naphthoquinone-esters showed a blue-shifted absorption maximum after the introduction of the two methoxy groups (See Table 19). All dyes exhibited absorption maxima perfectly fitting with the emission of LED emitting at 405 and 455 nm, except for the last set of naphthoquinones **(12)-(15)** for which blue shifted absorptions were found.

Table 19. Light absorption properties of the investigated compounds: maximum absorption wavelength (λ_{max}), molecular extinction coefficients at λ_{max}, 405 and 455nm.

PIs	λ_{max} (nm)	ε_{max} (M^{-1} cm^{-1})	ε_{405} (M^{-1} cm^{-1})	ε_{455} (M^{-1} cm^{-1})
(1)	330	500	260	30
(2)	380	1950	1500	90
(3)	382	1350	1070	100
(4)	378	1980	1510	40
(5)	383	970	810	100
(6)	388	2300	2010	260
(7)	383	2000	1670	130
(8)	382	1700	1360	170
(9)	387	1800	1550	210
(10)	385	1800	1630	570
(11)	388	2370	2110	360
(12)	333	3960	810	220
(13)	334	6110	1100	120
(14)	336	5700	960	70
(15)	339	4670	1290	360

Type I photoinitiating abilities of the studied compounds (0.5% w) were examined using RT-FTIR in thin (25 µm, in laminate) and thick (1.4 mm under air) samples after exposure to various LEDs (405 nm or 455 nm) using a benchmark monomer i.e. TA. Figure 27 depicts typical photopolymerization profiles, and Table 20 lists the final acrylate function conversions (FCs) that were attained.

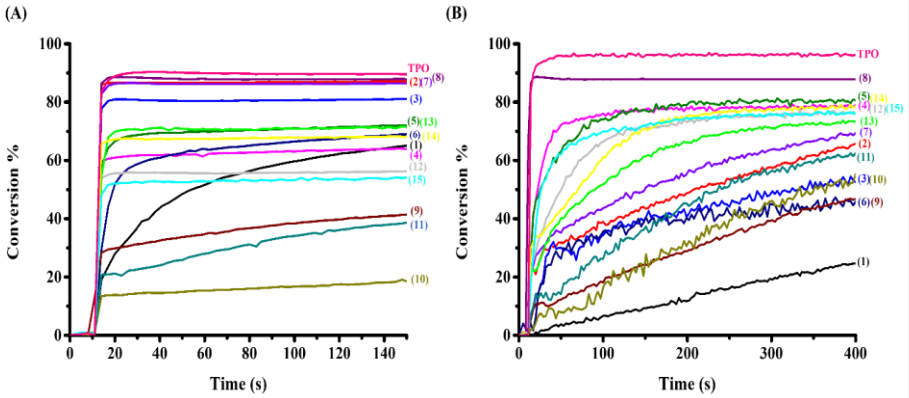

Figure 57. Photopolymerization profiles of TA (acrylate function conversion vs. irradiation time) using one component photoinitiating systems (0.5 % w) in (A) laminate (thickness = 25 µm) and (B) under air (thickness = 1.4 mm); the irradiation with LED (λ = 405 nm) starts at t = 10 s. Reproduced with the permission from Ref. [72].

By comparing compound **(1)** to the other structures (**2**–**15**) which all have ester groups, it is clear that the ester group is necessary for compound (**1**) to be able to react as a Type I photoinitiator. As commonly observed, compound **(8)** which has a methyl group on the carboxyl side achieved the highest FC of 88%, which is also very close to that obtained with the widely used photoinitiator TPO (See Figure 27 and Table 20). By comparing compounds with aryl substituents to those with alkyl substituents on the carboxyl side, it is clear that the alkyl substituted naphthoquinones exhibited higher photoinitiation performances (See Figure 27(A), as evidenced for compounds **(2)**, **(3)**, **(4)**, **(7)**, and **(8)** that exhibited rapid polymerization rates as well as high final conversions. If the methoxy groups were added onto the structures of naphthoquinones in order to improve their solubility in resins, unexpectedly, a severe reduction of the photoinitiating ability was evidenced. In fact, the ability of these compounds to initiate photopolymerization was greatly poorer than that of their analogues without methoxy groups (See compounds **(12)**, **(13)**, **(14)**, and **(15)** vs. compounds **(8)**, **(4)**, and **(7)** in Figure 27). Therefore, it is important to consider additional variables that may impact the ability to photopolymerize, such as the cleavage yields and the reactivity of the generated radicals. This clearly demonstrates that the photoinitiation ability of the studied compounds is not only associated to their light absorption properties.

Additionally, photopolymerization experiments were also carried out using a LED emitting at 455 nm in order to demonstrate the reactivity of the investigated structures at longer wavelengths. To the best of our knowledge, no oxime esters have been tested at such a

redshifted irradiation wavelength. The results notably demonstrated several naphthoquinone derivatives to exhibit a high photoinitiation performance, particularly for compounds **(8)**, **(2)**, **(3)**, **(4)**, and **(7)** (with alkyl substituents on the carboxyl side) (See Figure 28 and also Table 20). Even under LED@455 nm, compound **(8)** had the strongest reactivity, with a FC of 87% in thin samples and 84% in thick samples. When compared to commercial references such as the two-component system camphorquinone/ethyl dimethylaminobenzoate (CQ/EDB) (0.5%/0.5% w/w) or even Titanocene (Irgacure 784) (0.5% w) (see Figure 28 (A)), compound **(8)** could outperform these two reference systems, indicating that it could constitute a viable alternative to these benchmark photoinitiators. Comparatively, compounds **(9)**, **(10)**, **(11)**, **(12)** and **(15)** exhibited a reduced photoinitiating ability compared to the others, once again due to the fact that these esters are substituted with aromatic groups. To evidence the interest of compound **(8)** as a photoinitiator, the stability in resin was examined. The TA-based resin mixture containing 0.5% w compound (**8**) was stored without light and at room temperature for one month, and the photoinitiating effect was checked weekly. As can be seen in Figure 28 (B), a good storage stability was demonstrated without a significant decrease in performance.

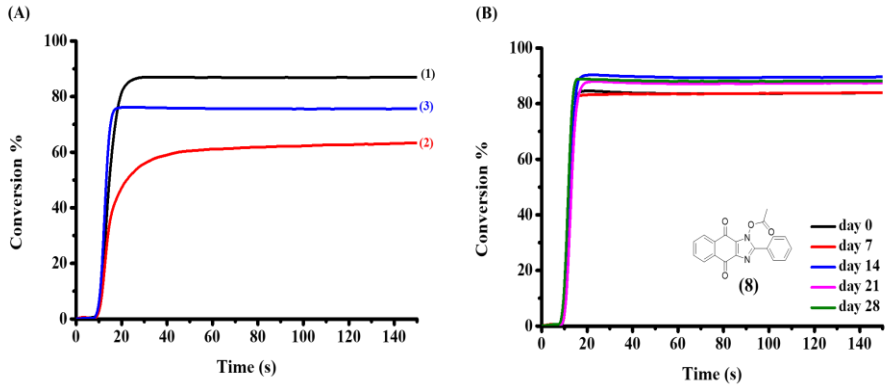

Figure 28. (A) Photopolymerization profiles of TA in laminate (thickness = 25 μm) of (1) compound **(8)** (0.5% w), (2) CQ/EDB (0.5%/0.5% w/w) and (3) Titanocene (0.5% w), upon exposure to a LED light (λ = 455 nm). **(B)** Photopolymerization profiles of TA using compound **(8)** (0.5% w) for different storage times in TA monomer. The irradiation starts at t = 10 s. Reproduced with the permission from Ref. [72].

Table 20. FCs using one component (0.5% w) photoinitiators after 100 s of irradiation with LED light (λ = 405 and 455 nm).

PIs	Thin Samples (25 µm) in laminate @405 nm	Thin Samples (25 µm) in laminate @455 nm	Thick Samples (1.4 mm) under air @405 nm	Thick Samples (1.4 mm) under air @455 nm
TPO	90%	61%	95%	77%
(1)	65%	48%	25%	1%
(2)	82%	80%	78%	78%
(3)	68%	71%	84%	81%
(4)	81%	83%	83%	85%
(5)	49%	55%	78%	74%
(6)	34%	53%	48%	68%
(7)	79%	76%	86%	80%
(8)	88%	87%	88%	84%
(9)	42%	24%	48%	65%
(10)	18%	32%	54%	54%
(11)	39%	32%	63%	66%
(12)	56%	65%	76%	78%
(13)	71%	73%	74%	78%
(14)	68%	59%	78%	61%
(15)	54%	48%	76%	67%

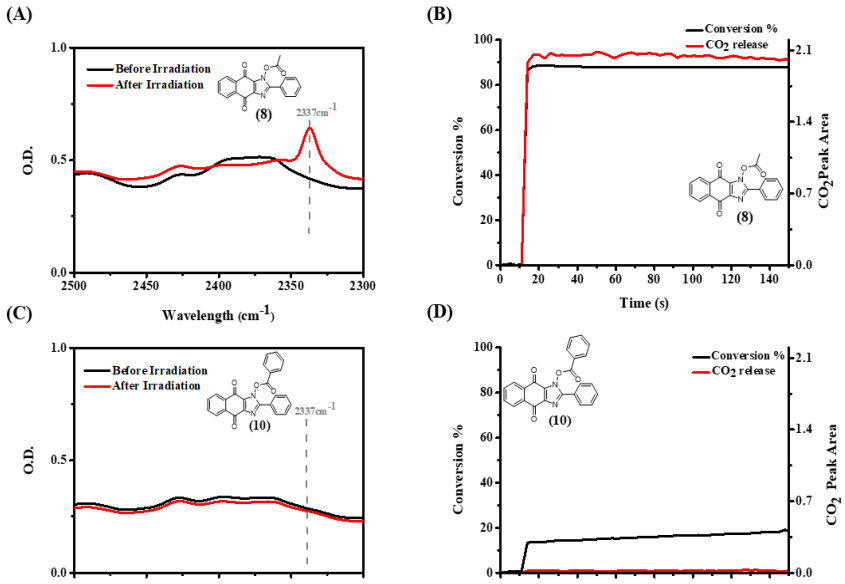

Figure 29. (A) Detection of CO_2 released during photopolymerization using **(8)**, **(B)** Decarboxylation-Conversion correlation using **(8)**, **(C)** Detection of CO_2 released during photopolymerization using **(10)** and **(D)** Decarboxylation-Conversion correlation using **(10);** PI (0.5% w) in TA (thin film polymerization @405nm in laminate). Reproduced with the permission from Ref. [72].

By FTIR, occurrence of a decarboxylation reaction could be clearly demonstrated for compound (**8**) in TA monomer when exposed to irradiation. For all derivatives bearing an alkyl group, such as compound **(8)**, appearance of a peak at 2337 cm^{-1} was detected after irradiation, demonstrating the release of CO_2 (See Figure 29 (A)). Derivatives with an aryl group, such as compound **(10)**, did not release CO_2, as shown in Figure 29 (C). Since the CO_2 release directly affects the polymerization efficiency (see Figures 29 (B) and (D) which highlight the connection between the two profiles), CO_2 release is primordial to get a high polymerization efficiency. A low radical launching efficiency is anticipated in the absence of CO_2 release.

For each of the studied compounds, the bond dissociation energy of the associated N-O bond (BDE) and the excited state energies (singlet and triplet excited state energies) could be determined by theoretical calculations and the results are listed in Table 21. From the singlet and triplet excited states where the dissociation enthalpies from the S_1 and T_1 states are negative and favorable, the N-O bond cleavage process is energetically favorable for the compounds **(2)** - **(11)**. Cleavage from the singlet state, however, is more advantageous because the ΔH values are lower. Compounds **(12)** - **(15)** did not have photoluminescence, so that the energy of the

singlet state could not be calculated. However, they have negative triplet enthalpy values, indicating that the cleavage is favorable from this energy state. Fluorescence lifetimes of the different naphthoquinone-based imidazolyl esters were also examined (See Table 21). Compound **(1)**, a derivative without ester functionality, had the longest lifetime of 3.45 ns, consistent with its photochemical results. Addition of the ester group resulted in shorter lifetimes, suggesting a cleavage from the S_1 state.

Table 21. Parameters characterizing the investigated naphthoquinone-based imidazolyl esters. Parameter calculated by molecular modelling: the bond dissociation energy BDE (N–O), the triplet state energy E_{T1}, the enthalpy ($\Delta H_{cleavageT1}$) for the cleavage process from T_1 ($\Delta H_{cleavageT1}$ = BDE – E_{T1}), the singlet excited state energy E_{S1} (evaluated from the experimental absorption and fluorescence spectra), the enthalpy ($\Delta H_{cleavageS1}$) for the cleavage process from S_1 ($\Delta H_{cleavageS1}$ = BDE - E_{S1}).

PIs	BDE (kcal/mol)	E_{S1} (kcal/mol)	τ_0 (S_1) (ns)	$\Delta H_{cleavageS1}$ (kcal/mol)	E_T (kcal/mol)	$\Delta H_{cleavageT1}$ (kcal/mol)
(1)	41.78	62.3	3.45	-20.51	50.98	-9.2
(2)	35.76	63.5	2.49	-27.74	50.57	-14.81
(3)	36.54	63.8	2.46	-27.26	50.69	-14.15
(4)	34.95	63.5	1.76	-28.55	50.76	-15.81
(5)	34.90	62.2	2.75	-27.3	50.77	-15.87
(6)	34.94	62.6	2.63	-27.66	50.76	-15.82
(7)	35.03	62.8	3.09	-27.77	50.53	-15.50
(8)	36.19	65.13	2.36	-28.94	50.71	-14.52
(9)	34.92	64.3	2.41	-29.38	50.47	-15.55
(10)	34.87	61.8	2.56	-26.93	50.75	-15.88
(11)	34.78	62.6	2.57	-27.82	50.77	-15.99
(12)	32.68	-	-	-	47.12	-14.44
(13)	32.38	-	-	-	47.56	-15.18
(14)	31.41	-	-	-	47.29	-15.88
(15)	31.89	-	-	-	47.82	-15.93

Compound **(8)** (with a methyl substituent in the carboxyl side) in this new family of naphthoquinone-based imidazolyl ester structures exhibited excellent photoinitiating performance so that it could replace well-established references such as TPO as photoinitiator.

7.2. *N*-naphthalimide Ester Derivatives

Naphthalimide-based PIs have been the subject of many chemical modifications during the last decade. Different substituents were notably introduced to finely tune the absorption properties of naphthalimide derivatives. Noticeably, until 2020, naphthalimide derivatives were

only investigated to elaborate two- and three-component photoinitiating systems. Besides, some works were also devoted to design naphthalimides usable as monocomponent photoinitiating systems. [73-75] In a recent study by Lalevée and coworkers, 2,6-dioxopiperidin-1-yl esters were prepared with naphthalimides. Irradiation could lead to the homolytic cleavage of the N-O bond, allowing the acyloxy or the aryloxy groups to undergo a decarboxylation process and produce an alkyl radical.[75] These free radicals could initiate the polymerization of monomers. Nine *N*-naphthalimide esters (**NPIE1**-**NPIE9**) were examined as Type I photoinitiators. To maximize the photocleavage efficiency, various cleavable groups were linked directly to the chromophore using the oxime ester group. For comparison, a second series of naphthalimide derivatives was also prepared, in which the oxime ester group was separated from the chromophore by mean of an aliphatic spacer. This second series of oxime esters was found to be almost incapable to initiate a polymerization, demonstrating the critical importance of the distance between the photocleavable group and the light absorbing chromophore.

The different naphthalimide-based photoinitiators **NPIE1**-**NPIE9** were prepared in three steps, starting from 6-bromo-1*H*,3*H*-benzo[*de*]isochromene-1,3-dione **1**. First, in basic conditions, 6-(octylthio)-1*H*,3*H*-benzo[*de*]isochromene-1,3-dione **2** could be produced in 87% yield by nucleophilic substitution with octanethiol. Then, using sodium acetate and hydroxylamine hydrochloride, oxime **3** could be obtained in 98% yield. Finally, using triethylamine as the base and the proper acid chloride, esterification of the oxime group could be obtained. According to Scheme 10, the reaction yields for **NPIE1**-**NPIE9** ranged from 71% for **NPIE9** to 93% for **NPIE7**. In the end, **NPIMO** was prepared as a control substance. Indeed, **NPIMO** is not an oxime ester due to its alkylation with iodomethane. Starting from **3**, this compound could be obtained in 85% yield.

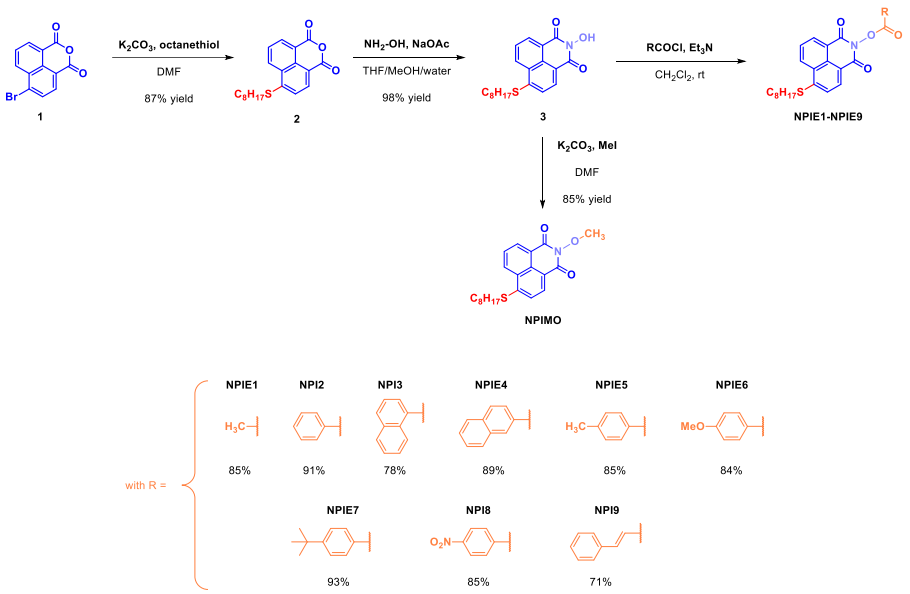

Scheme 10. Synthetic routes to **NPIE1-NPIE9** and **NPIMO**.

A second series of molecules, **NO1-NO8**, was created to examine the impact of the distance introduced between the chromophore and the cleavable group (See Scheme 11). By using an excess of ethylenediamine and 4-fluoroacetophone **4**, 1-(4-((2-aminoethyl)amino)phenyl)ethan-1-one **5** could be produced in 88% yield. Then, after two days of reaction in 2-ethoxyethanol, 2-(2-((4-acetylphenyl)amino)ethyl)-6-(octylthio)-1*H*,3*H*-benzo[*de*]isochromene-1,3-dione **6** was produced in 82% by condensation on 6-(octylthio)-1*H*,3*H*-benzo[*de*]isochromene-1,3-dione with 1-(4-((2-aminoethyl)amino)phenyl)ethan-1-one **5**. The oxime could be obtained by reacting the ketone **6** with sodium acetate, hydroxylamine hydrochloride in a mixture of solvents. 2-(2-((4-(1-(Hydroxyimino)ethyl)phenyl)amino)ethyl)-6-(octylthio)-1*H*-benzo[*de*]isoquinoline-1,3(2*H*)-dione **7** was obtained in 96% yield. Oxime esters were prepared by following a similar process to that used for **NPIE1-NPIE9**. Reaction yields ranged from 62% for **NO2** to 75% for **NO7** respectively.

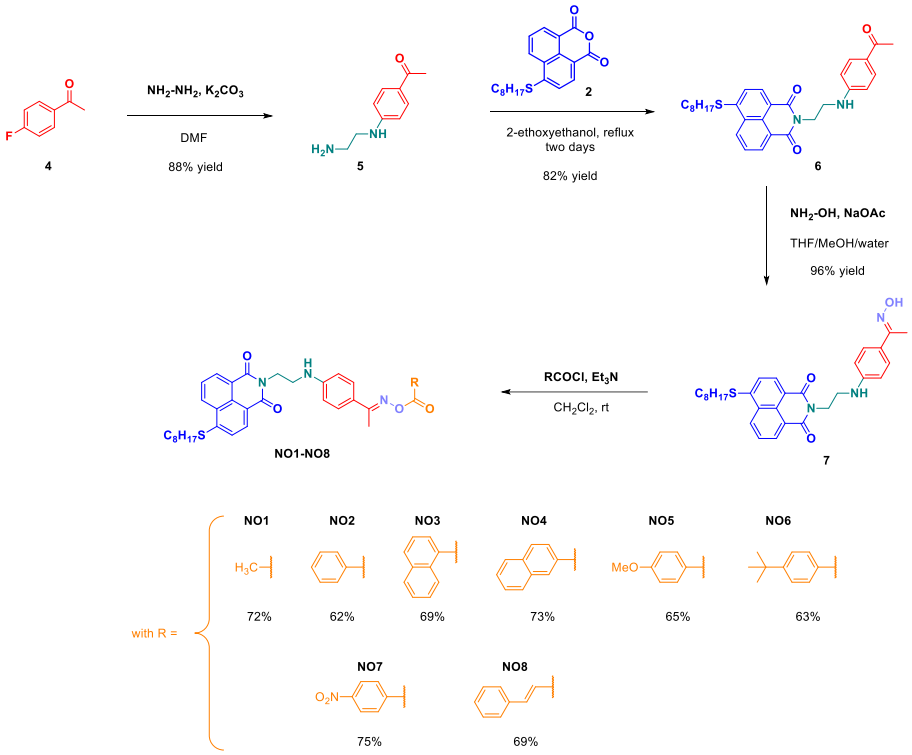

Scheme 11. Synthetic routes to **NO1-NO8**.

Figure 30 shows the UV-visible absorption spectra of PIs in acetonitrile, and Table 22 lists the main characteristics concerning the light absorption properties of the various PIs. The maximum absorption wavelength of **NPIMO** (λ_{max}) was 394 nm. The maximum absorption wavelengths of **NPIE**s were slightly redshifted in comparison to **NPIMO**. All **NPIE**s maximum absorption wavelengths were between 397 nm and 398 nm. These results clearly show that the substituents attached to the ester group have only little influence on the light absorption properties of **NPIEs**. Interestingly, molar extinction coefficients of **NPIE**s determined at 405 nm ($\varepsilon_{405\ nm}$), such as $\varepsilon_{405\ nm}$(**NPIE1**) = 15000 $M^{-1}cm^{-1}$ and $\varepsilon_{405\ nm}$ (**NPIE2**) = 14400 $M^{-1}cm^{-1}$ were favorable for polymerization experiments carried out at 405 nm.

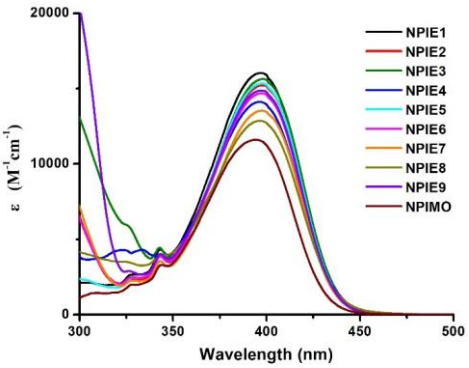

Figure 30. UV-visible absorption spectra of **NPIE**s and **NPIMO** in acetonitrile. Reproduced with permission of Ref. [76]

The high molar extinction values of the different dyes at 405 nm allowed the authors to examine the photoinitiation performance of **NPIE**s in free radical photopolymerization. Figure 31a depicts the polymerization profiles of TMPTA (acrylate conversion vs. irradiation duration. Under LED@405 nm, NPIEs showed good photoinitiation capabilities during free radical polymerization. Interestingly, even though the TPO system had a reasonably quick polymerization rate, the acrylate function conversion of TMPTA in the presence of **NPIE1** (FC = 68%) was higher than that of the benchmark structure TPO (FC = 66%).

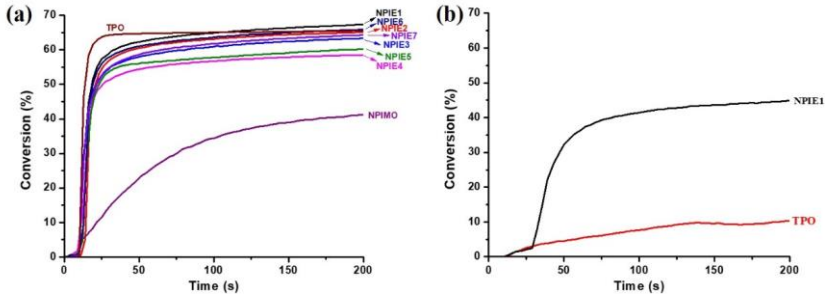

Figure 31. Photopolymerization profiles of TMPTA in laminate (~25 μm) in the presence of photoinitiators (2×10^{-5} mol/g TMPTA) (a) upon exposure to a LED@405 nm; (b) upon exposure to a LED@455 nm. The irradiation starts at t = 10 s. Reproduced with permission of Ref. [76]

Furthermore, **NPIE7** demonstrated a good photoinitiating ability (FC = 66%). When exposed to a LED@405 nm while **NPIMO** (without ester group) was present, a function

conversion of 41% was determined. It suggests that the ester group plays a crucial role in these PIs structural composition. Upon exposure to a LED@455 nm, the photoinitiation capacity of **NPIE1** and TPO was also examined (See Figure 31b). TPO proved to be almost ineffective to initiate a polymerization upon irradiation at 455 nm. Significantly, the ultimate functional conversion of TMPTA in the presence of **NPIE1** was 44%, which benefited from the efficient absorption of visible light by **NPIE1** (much better absorption than TPO at 455 nm).

The singlet excited state energy (E_{S1}) could be determined at the intersection of the UV-visible absorption and fluorescence emission spectra of **NPIE**s. From computational methods, the triplet state energy (E_T) and the dissociation energy of the N-O bond of **NPIE**s were estimated. Table 23 contains the N-O bond cleavage enthalpies of the singlet state (S_1) and triplet state (T_1). The results ($\Delta H_{cleavage\ S1} < 0$, $\Delta H_{cleavage\ T1} > 0$) indicate that the major pathway involves cleavage of the N-O bond from the singlet state. Additionally, a time-correlated single-photon counting system was used to evaluate the fluorescence lifetimes of PIs in acetonitrile. Table 23 lists the fluorescence lifetimes (τ_0) of PIs. In accordance with the favorable values of cleavage S_1 for the N-O bond cleavage process from the singlet excited state, **NPIE**s have shorter fluorescence lifetimes than **NPIMO**.

Table 23. Some parameters characterizing the cleavage process of the N−O bond.

NPIEs	N−O BDE (kcal.mol^{-1})	E_{S1} (kcal.mol^{-1})	$\Delta H_{cleavage\ S1}$[a] (kcal.mol^{-1})	E_T (kcal.mol^{-1})	$\Delta H_{cleavage\ T1}$ (kcal.mol^{-1})	τ_0 (ns)
NPIE1	63.17	65.72	-2.55	50.63	12.54	6.09
NPIE2	62.00	65.49	-3.49	50.68	11.32	5.89
NPIE3	61.85	65.58	-3.73	50.67	11.18	5.75
NPIE4	61.94	65.43	-3.49	50.69	11.25	5.69
NPIE5	61.91	65.66	-3.75	50.73	11.18	5.80
NPIE6	61.87	65.51	-3.64	50.79	11.08	5.70
NPIE7	61.98	65.63	-3.65	50.76	11.22	5.71
NPIE8	61.41	65.36	-3.95	50.52	10.89	5.30
NPIE9	63.06	65.61	-2.55	50.79	12.27	5.62
NPIMO	–	–	–	–	–	6.72

[a] $\Delta H_{cleavage\ S1/T1} = BDE(N{-}O) - E_{S1}/E_T$

Interestingly, photodecomposition of oxime esters upon irradiation could be monitored

by RT-FTIR by following the formation of CO_2 during the decarboxylation reaction. Here, photopolymerization experiments involving the decomposition of **NPIE**s in TMPTA after exposure to a LED@405 nm were also examined using RT-FTIR. Figures 32a and 32b demonstrate that following irradiation, an emerging absorption peak at 2337 cm^{-1} was found in the infrared spectra of the **NPIE1**/TMPTA and **NPIE2**/TMPTA systems. The generated peak was attributed to CO_2. Infrared spectra of the **NPIMO**/TMPTA (Figure 32c) and TPO/TMPTA systems did not have this peak. According to these findings, irradiation can induce a decarboxylation reaction for both alkoxy or aryloxy radicals, subsequent to photocleavage. Absorbance of **NPIE1** and **NPIE2** during the photolysis tests remains unchanged, evidencing the photostability of the naphthalimide moiety. Figure 32d illustrates that during the photopolymerization process, intensity of the CO_2 absorption peak for the **NPIE1**/TMPTA system was higher than that of the **NPIE2**/TMPTA system, indicating that more CO_2 was released by the **NPIE1**/TMPTA system. These results demonstrate that the acetoxy group, which is also present in **NPIE1**, can undergo an easier decarboxylation reaction than the benzoyloxy group.

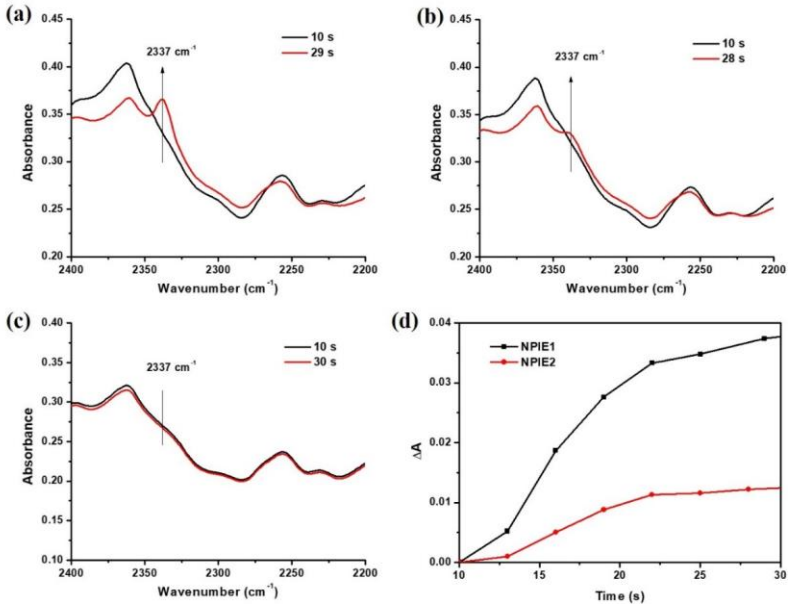

Figure 32. Infrared spectra of PI/TMPTA in photopolymerization experiments at different times (a) **NPIE1**/TMPTA; (b) **NPIE2**/TMPTA; (c) **NPIMO**/TMPTA; (d) The curve of absorption intensity of CO_2 obtained with the **NPIE1**/TMPTA and **NPIE2**/TMPTA systems ($A = A_t - A_0$, where A_t is the absorbance intensity at t s; A_0 is the absorbance intensity before irradiation (at t = 10 s)). Reproduced with permission of Ref. [76]

Based on the above findings, **NPIE**s used as Type I PIs may have a chemical mechanism similar to that depicted in Scheme 9. Molecules may be promoted in their excited states upon irradiation of **NPIE**s. The naphthalimide and alkyloxy/aryloxy radicals are produced by a fast cleavage of the N-O bond from the singlet state. Active radicals used during the free radical polymerization of monomers can then be produced by decarboxylation of the alkyloxy/aryloxy radicals. Photoinitiation ability of **NPIE**s is significantly influenced by the substituents R. The production of methyl radicals was facilitated by the efficient decarboxylation of acetyloxy radicals. Thus, among them, the **NPIE1** system showed the highest monomer conversion. The **NPIE7** system was found to have a slightly higher initiation ability than the others. The addition reaction of the electron-deficient double bond of acrylate is facilitated by the radicals produced with electron-rich isopropyl groups. In **NPIE4**/TMPTA and **NPIE8**/TMPTA, the CO_2 peak was not observed, which could be attributed to an unfavorable cleavage or decarboxylation process. Therefore, with these two systems, low monomer conversions were obtained. In addition, the naphthalimide chromophore-based complexes are capable of undergoing a hydrogen abstraction reaction to produce radicals, resulting in the conversion of TMPTA to a low function state in the presence of **NPIMO**. Therefore, photoinitiating ability of **NPIMO** can be assigned to Type II behavior.

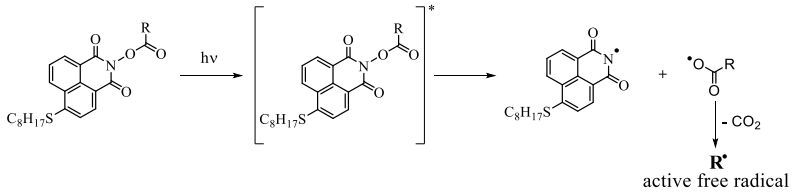

Scheme 12. Proposed chemical mechanism of **NPIE**s as Type I PIs.

Another molecule, **NO1** (See structure in Scheme 11), was prepared in parallel to the **NPIE1**-**NPIE9** series in order to examine the impact of the separation between the chromophore and the photocleavable group. As shown in Figure 33a, **NO1** had a higher molar extinction coefficient at 405 nm than **NPIE1**, and its maximum absorption wavelength was blue-shifted relative to **NPIE1** (λ_{max} = 397 nm). Figure 33b shows the photopolymerization of TMPTA in the presence of **NO1** when exposed to an LED at 405 nm. Compared to **NO1**, **NPIE1** displayed a substantially greater capacity for photoinitiation. The naphthalimide chromophore is still responsible from the absorption of **NO1** light absorption band, with a maximum absorption located at ca 397 nm. The spacer in the **NO1** structure prevents the energy from being transferred to the oxime ester group when the naphthalimide moiety in the structure is

excited by a LED@405nm. No active radicals are produced during the oxime ester group's cleavage process; in contrast to **NPIE1**, no CO_2 peak was detected for **NO1**, indicating that the cleavage mechanism is not advantageous for **NO1**. As a result, TMPTA had a low function conversion (38%) when **NO1** was used as the photoinitiator. With a spacer between the chromophore and the cleavable ester moiety, the other naphthalimide-esters (noted **NO2**-**NO8**) exhibited a similar reactivity. Low performance levels are observed, which is consistent with a deficiency in energy transfer. The outcomes further show that NPIEs with the ester group in close vicinity to the naphthalimide chromophore is an important structural parameter in order to optimize the energy transfer efficiency upon photoexcitation.

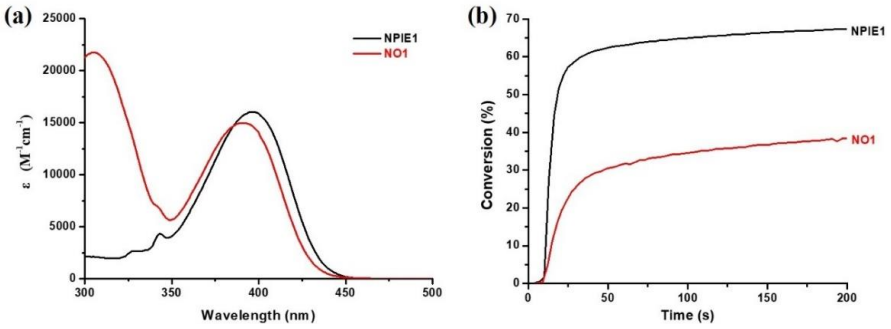

Figure 33. (a) UV-visible absorption spectra of **NPIE1** and **NO1**; (b) Photopolymerization profiles of TMPTA in laminate (~25 μm) upon exposure to a LED@405 nm in the presence of **NPIE1** and **NO1** (2×10^{-5} mol/g TMPTA). The irradiation starts at t = 10 s. Reproduced with permission of Ref. [75]

8. Chromophore effects on photoinitiation ability

In general, as shown by the different studies performed so far, an important number of parameters such as the absorption properties, the efficiency of the photocleavage and the decarboxylation abilities, as well as the reactivity of the generated radicals, can drastically affect the overall mechanism of decomposition of oxime esters and in turn the final monomer conversion (See Scheme 13). In this part, the effect of the choice of the chromophore with regards to these different parameters is presented for the first time.

Scheme 13. Key steps in OXE photoinitiation efficiency.

8.1. Absorption properties

Absorption properties of the photoinitiator (PI) are mainly controlled by its chemical structure, including the different groups attached to the chromophore. These groups can determine the position of the absorption spectra on the electromagnetic spectrum. Therefore, the wavelengths that a photoinitiator can absorb are reflected in an absorption spectrum. In addition, the absorption characteristics associated with the photosensitive molecule are revealed by the absorbance of the dye at a specific wavelength. In this review, each chromophore was chosen to shift the absorption wavelength of the oxime ester-based photoinitiators into the visible range. As summarized above, a wide range of chromophores have been examined during the last three years including triphenylamine, coumarin, carbazole, pyrene, anthracene, phenothiazine and other analogues derivatives... The different results have demonstrated that all the proposed structures exhibited good absorption properties in the visible range. Especially, all chromophores are adapted for light irradiation done at 405 nm, which is a standard wavelength for 3D printers. The following table summarizes the absorption properties for all the chromophores.

Table 22. Light absorption properties with different chromophore.

Chromophore	λ_{max} (nm)	ε_{max} ($M^{-1}cm^{-1}$)	$\varepsilon_{405\ nm}$ ($M^{-1}cm^{-1}$)
Triphenylamine	370 ↔ 380	30000 ↔ 45000	13000 ↔ 18000
Coumarin	430 ↔ 435	28000 ↔ 50000	16500 ↔ 25500
Carbazole	370 ↔ 380	12000 ↔ 20000	1200 ↔ 5400
Pyrene	360 ↔ 365	22000 ↔ 52000	535 ↔ 6400
Anthracene[1]	370 ↔ 375		
Phenothiazine	320 ↔ 350	6000 ↔ 6700	680 ↔ 2700

[1]: see Figure 24 for absorption of An-OXE 2 as example.

The results show that coumarin-based photoinitiators exhibit the highest absorption properties compared to the other chromophores especially when exposed to irradiation done at 405 nm. The trend of efficiency for the absorption properties at 405 nm respects the following order: **Coumarin** > **Triphenylamine** > **Carbazole** > **Pyrene** > **Phenothiazine** > **Anthracene**. This can partially explain the photopolymerization results, but other factors may also have an effect on the photoinitiating ability of the investigated photoinitiators to initiate reactions.

8.2. Cleavage reaction

The usual cleavage in the oxime ester is mainly expected from the triplet state (T_1), but depending on the structure of the OXE, cleavage from the singlet state (S_1) has also been suspected (See Scheme 14). Table 23 summarizes the (N-O) bond dissociation energy and the cleavage process enthalpies from various excited state levels (S_1 or T_1) ($\Delta H_{cleavage\ S1\ or\ T1}$ = BDE(N-O) – $E_{(S1\ or\ T1)}$) for the various oxime esters.

Table 23. Some parameters characterizing the cleavage process of the N–O bond.

Chromophore	N–O BDE (kcal mol^{-1})	$\Delta H_{cleavage\ S1}$[a] (kcal mol^{-1})	$\Delta H_{cleavage\ T1}$[a] (kcal mol^{-1})	τ_0 (ns)
Triphenylamine	53 ↔ 57	-14.5 ↔ -21.25	-0.3 ↔ -8.5	1.25 ↔ 1.5
Coumarin	42 ↔ 50.5	-17 ↔ -10.6	-5 ↔ 6	1.6 ↔1.9
Carbazole	41 ↔ 44	-32.5 ↔ -26.5	-21 ↔ -5	1.4 ↔ 3.85
Pyrene	43 ↔ 47	-23.85	4 ↔ 6	2.5 ↔ 4
Anthracene	41 ↔ 48	-21.5	5 ↔ 12.5	1.5 ↔ 4.5
Phenothiazine	54 ↔ 54.5	-9 ↔ -11	5.6	7 ↔ 7.65

[a]$\Delta H_{cleavage\ S1/T1}$ = BDE(N–O) – E_{S1}/E_{T1}

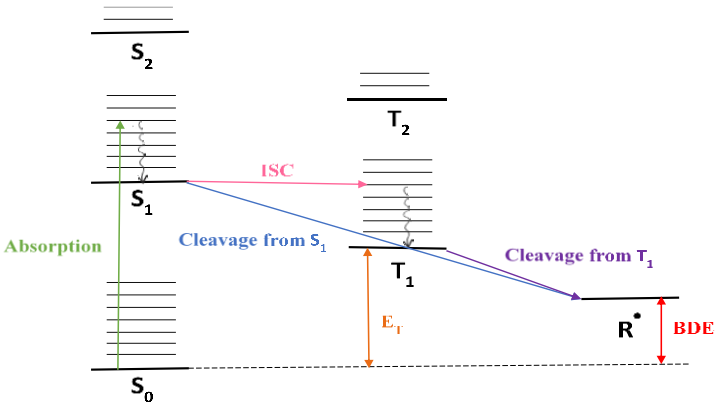

Scheme 14. Jablonski Diagram for cleavage from either S_1 or T_1.

As we can see in Table 24, the cleavage from S_1 is favorable for all chromophores in the following order: **Carbazole** > **Pyrene** > **Anthracene** > **Triphenylamine** > **Coumarin** > **Phenothiazine**. In addition, for some chromophores such as **Carbazole**, **Coumarin**, and **Triphenylamine**, the possibility of cleavage from T_1 is also energetically favorable.

8.3. Photoinitiation behavior

All the investigated chromophores showed a significant shift towards the visible and consequently a good efficiency in photopolymerization process under LED@405 nm, the associated final acrylate conversions (FCs) are summarized in Table 24 with a trend: **Carbazole** > **Triphenylamine** > **Coumarin** and > **Pyrene** > **Phenothiazine** > **Anthracene**.

Commenté [DF2]: Visiblement, il manque une famille

Table 24. Final acrylate function conversion (FCs) after 100 s of irradiation with LED light (λ = 405 nm) in laminate.

Chromophore	Final acrylate function conversion (FCs) Thin sample (25 µm) in laminate
Triphenylamine	35% ↔ 75% [a]
Coumarin	35% ↔ 75% [a]
Carbazole	35% ↔ 85% [a]
Pyrene	15% ↔ 80% [b]
Anthracene	0% ↔ 50% [b]
Phenothiazine	15% ↔ 55% [b]

[a]TMPTA based system

[b]TA based system

Other factors such as the decarboxylation reactions can also have a significant effect on the efficiency as shown in the previously published papers. For example, the decarboxylation is more favorable when alkyl substituents are involved compared to aryl substituents (see previous results), in addition the reactivity of the generated radicals to initiate the polymerization.

9. Conclusion

The design of oxime esters is an active field of research, for which several types of chromophores were examined during the last three years in order to shift the absorption wavelength of these dyes towards the visible range. An overview of the recently proposed structures is given in this review. According to the investigations, different factors including absorption properties, cleavage mechanisms, decarboxylation reactions, and the reactivity of the generated radicals can drastically influence the initiation abilities of oxime esters. In order to select the optimal structures that can act as Type I photoinitiators, it was demonstrated how the chromophore coupled to the oxime ester structure can drastically affect the final monomer conversion. Furthermore, in order to find the radicals that can produce the most efficient polymerization reactions, there is still much work to be done. Indeed, there is a wealth of literature on aromatic and heterocyclic radicals. In addition, current research has conclusively shown that the methyl radicals were the most reactive ones ever described in the literature for oxime esters. Future research on novel oxime esters will focus on the generation of aliphatic radicals that could considerably improve the polymerization efficiency. The excited state involved in the photocleavage of oxime esters is another factor to take into account while designing oxime esters. In fact, compared to dyes for which a triplet pathway is found, recent investigations have shown that the singlet deexcitation pathway improves the photocleavage efficiency as well as the monomer conversion.

10. References

[1] P. Garra, C. Dietlin, F. Morlet-Savary, F. Dumur, D. Gigmes, J.P. Fouassier, J. Lalevée, Photopolymerization processes of thick films and in shadow areas: a review for the access to composites, Polymer Chemistry, 2017, 8.46, 7088-7101.

[2] J. P. Fouassier, J. Lalevée, Photoinitiators: Structures, Reactivity and Applications in Polymerization, Wiley, Weinhein, 2021.

[3] J. P. Fouassier, Photoinitiation, Photopolymerization, and Photocuring: Fundamentals and Applications, Hanser Publishers, New York 1995.

[4] Y. Yagci, S. Jockusch, N. J. Turro, Photoinitiated polymerization: advances, challenges, and opportunities, Macromolecules, 2010, 43, 6245-6260.

[5] J. Lalevée, J. P. Fouassier, Dye Photosensitized Polymerization Reactions: Novel Perspectives, RSC Photochemistry Reports, Ed. A. Albini, E. Fasani, Photochemistry, London, UK, 2015, 215–232.

[6] K. Dietliker, T. Jung, J. Benkhoff, H. Kura, A. Matsumoto, H. Oka, D. Hristova, G. Gescheidt, G. Rist, New developments in photoinitiators, Macromolecular Symposia. Weinheim : WILEY-VCH Verlag, 2004. 217.1, 77-98.

[7] M. A. Tehfe, F. Dumur, B. Graff, F. Morlet-Savary, D. Gigmes, J. P. Fouassier, J. Lalevée, Design of new Type I and Type II photoinitiators possessing highly coupled pyrene–ketone moieties, Polymer Chemistry, 2013, 4.7, 2313-2324.

[8] A. Kowalska, J. Sokolowski, K. Bociong, The photoinitiators used in resin based dental composite—a review and future perspectives, 2021, Polymers, 13.3, 470.

[9] M. Abdallah, D. Magaldi, A. Hijazi, B. Graff, F. Dumur, J.P. Fouassier, T.T. Bui, F. Goubard, J. Lalevée, Development of New High-Performance Visible Light Photoinitiators Based on Carbazole Scaffold and Their Applications in 3D Printing and Photocomposite Synthesis, J. Polym. Sci., Part A, 2019, 57, 2081–2092.

[10] J. Lalevée, H. Mokbel, J.-P. Fouassier, Recent Developments of Versatile Photoinitiating Systems for Cationic Ring Opening Polymerization Operating at Any Wavelengths and under Low Light Intensity Sources, Molecules, 2015, 20, 7201–7221.

[11] P. Xiao, F. Dumur, B. Graff, J.P. Fouassier, D. Gigmes, J. Lalevée, Cationic and Thiol-Ene Photopolymerization upon Red Lights Using Anthraquinone Derivatives as Photoinitiators, Macromolecules, 2013, 46, 6744–6750.

[12] C. Dietlin, S. Schweizer, P. Xiao, J. Zhang, F. Morlet-Savary, B. Graff, J. P Fouassier, J. Lalevée, Photopolymerization upon LEDs: new photoinitiating systems and strategies, Polymer Chemistry, 2015, 6.21, 3895-3912.

[13] X. Peng, D. Zhu, P. Xiao, Naphthoquinone derivatives: Naturally derived molecules as blue-light-sensitive photoinitiators of photopolymerization, European Polymer Journal, 2020, 127, 109569.

[14] M. M. Abdul-Monem, Naturally Derived Photoinitiators for Dental and Biomaterials Applications, European Dental Research and Biomaterials Journal, 2020, 1.02, 72-78.

[15] C.-H. Chen, Y. Wang, T. Michinobu, S.-W. Chang, Y.-C. Chiu, C.-Y. Ke, G.-S. Liou, Donor–Acceptor Effect of Carbazole-Based Conjugated Polymer Electrets on Photoresponsive Flash Organic Field-Effect Transistor Memories, ACS Appl. Mater. Interfaces, 2020, 12, 6144–6150.

[16] A. Bagheri, J. Jin, Photopolymerization in 3D Printing, ACS Appl. Polym. Mater, 2019, 1, 593–611.

[17] M. Topa, J. Ortyl, Moving Towards a Finer Way of Light-Cured Resin-Based Restorative Dental Materials: Recent Advances in Photoinitiating Systems Based on Iodonium Salts, Materials, 2020, 13, 4093.

[18] E. Andrezajewska, K. Grajek, Recent advances in photo-induced free-radical polymerization, MOJ Polym Sci, 2017, 1, 58–60.

[19] F. Yoshino, A. Yoshida, Effects of blue-light irradiation during dental treatment, Jpn Dent Sci Rev, 2018, 54, 160–168.

[20] H. Arikawa, H. Takahashi, T. Kanie, S. Ban, Effect of various visible light photoinitiators on the polymerization and color of light-activated resins, Dental Materials Journal, 2009, 28, 454–460.

[21] N. Corrigan, J. Yeow, P. Judzewitsch, J. Xu, C. Boyer, Seeing the Light: Advancing Materials Chemistry through Photopolymerization, Angewandte Chemie International Edition, 2019, 58, 5170–5189.

[22] M. Schmitt, Synthesis and testing of ZnO nanoparticles for photo-initiation: Experimental observation of two different non-migration initiators for bulk polymerization, Nanoscale, 2015, 7, 9532-9544.

[23] E. Vessally, H. Saeidian, A. Hosseinian, L. Edjlali, A. Bekhradnia, A review on synthetic applications of oxime esters, Current Organic Chemistry, 2017, 21.3, 249-271.

[24] D. Wang, S. Ren, H. Wang, H. Yan, J. Feng, X. Zhang, Semisynthesis and antifungal activity of novel oxime ester derivatives of carabrone modified at C (4) against Botrytis cinerea, Chemistry & biodiversity, 2014, 11.6, 886-903.

[25] J. Xu, G. Ma, K. Wang, J. Gu, S. Jiang, J. Nie, Synthesis and photopolymerization kinetics of oxime ester photoinitiators, Journal of Applied Polymer Science, 2012, 123.2, 725-731.

[26] Y. Gao, J. Song, S. Shang, D. Wang, J. Li, Synthesis and antibacterial activity of oxime esters from dihydrocumic acid, BioResources, 2012, 7.3, 4150-4160.

[27] B. Kraeutler, C. D. Jaeger, A. J. Bard, Direct Observation of Radical Intermediates in Photo-Kolbe Reaction - Heterogeneous Photocatalytic Radical Formation by Electron-Spin Resonance, J. Am. Chem. Soc, 1978, 100.15, 4903-4905.

[28] W. Qiu, J. Zhu, K. Dietliker, Z. Li, Polymerizable Oxime Esters: An Efficient Photoinitiator with Low Migration Ability for 3D Printing to Fabricate Luminescent Devices, ChemPhotoChem, 2020, 4.11, 5296-5303.

[29] D. E. Fast, A. Lauer, J. P. Menzel, A. M. Kelterer, G. Gescheidt, C. Barner-Kowollik, Wavelength-Dependent Photochemistry of Oxime Ester Photoinitiators, Macromolecules, 2017, 50, 1815-1823.

[30] F. Dumur, Recent advances on visible light Triphenylamine-based photoinitiators of polymerization. European Polymer Journal, 2022, 111036.

[31] D. Ladika, G. Noirbent, F. Dumur, D. Gigmes, A. Mourka, M. G. D. Barmparis, M. Farsari, and D. Gray, Synthesis and application of triphenylamine-based aldehydes as photo-initiators for multi-photon lithography. Applied Physics A, 2022, 128(9), 1-8.

[32] M. Abdallah, F. Dumur, B. Graff, A. Hijazi, J. Lalevée, High performance dyes based on triphenylamine, cinnamaldehyde and indane-1, 3-dione derivatives for blue light induced polymerization for 3D printing and photocomposites, Dyes and Pigments, 2020, 182, 108580.

[33] Y. H. Li, Y. C. Chen, Triphenylamine-hexaarylbiimidazole derivatives as hydrogen-acceptor photoinitiators for free radical photopolymerization under UV and LED light, Polymer Chemistry, 2020, 11.8, 1504-1513.

[34] S. C. Yen, Z. H. Lee, J. S. Ni, C. C. Chen, Y. C. Chen, Effect of number and position of methoxy substituents on triphenylamine-based chalcone visible-light-absorbing photoinitiators, Polymer Chemistry, 2022.

[35] Z.H. Lee, F. Hammoud, A. Hijazi, B. Graff, J. Lalevée, Y.C. Chen, Synthesis and free radical photopolymerization of triphenylamine-based oxime ester photoinitiators, Polymer Chemistry, 2021, 12, 1286-1297.

[36] F. Hammoud, Z.H. Lee, B. Graff, A. Hijazi, J. Lalevée, Y.C. Chen, Novel phenylamine-based oxime ester photoinitiators for LED-induced free radical, cationic, and hybrid polymerization, Journal of Polymer Science, 2021, 59, 1711–1723.

[37] F. Dumur, Recent advances on coumarin-based photoinitiators of polymerization, European Polymer Journal, 2021, 110962.

[38] M. Rahal, B. Graff, J. Toufaily, T. Hamieh, F. Dumur, J. Lalevée, Design of keto-coumarin based photoinitiator for Free Radical Photopolymerization: Towards 3D printing and photocomposites applications, European Polymer Journal, 2021, 154, 110559.

[39] M. Abdallah, A. Hijazi, J. T. Lin, B. Graff, F. Dumur, J. Lalevée, Coumarin derivatives as photoinitiators in photo-oxidation and photo-reduction processes and a kinetic model for simulations of the associated polymerization profiles. ACS Applied Polymer Materials, 2020, 2.7, 2769-2780.

[40] Z. Li, X. Zou, G. Zhu, X. Liu, R. Liu, Coumarin-based oxime esters: photobleachable and versatile unimolecular initiators for acrylate and thiol-based click photopolymerization under visible light-emitting diode light irradiation., ACS applied materials & interfaces, 2018, 10.18, 16113-16123.

[41] W. Qiu, M. Li, Y. Yang, Z. Li, K. Dietliker, Cleavable coumarin-based oxime esters with terminal heterocyclic moieties: photobleachable initiators for deep photocuring under visible LED light irradiation. Polymer Chemistry, 2020, 11.7: 1356-1363.

[42] F. Hammoud, N. Giacoletto, G. Noirbent, B. Graff, A. Hijazi, M. Nechab, D. Gigmes, F. Dumur, J. Lalevée, Substituent Effects on Photoinitiation Ability of Coumarin-Based Oxime Ester Photoinitiators for Free Radical Photopolymerization, Materials Chemistry Frontiers, 2021.

[43] J. Barth, M. Buback, P. Hesse, T. Sergeeva, Termination and Transfer Kinetics of Butyl Acrylate Radical Polymerization Studied via SP-PLP-EPR. Macromolecules 2010, 43.9, 4023-4031.

[44] F. Dumur, Recent advances on carbazole-based photoinitiators of polymerization. European Polymer Journal, 2020, 125, 109503.

[45] F. Dumur, Recent advances on carbazole-based oxime esters as photoinitiators of polymerization, European Polymer Journal, 2022, 111330.

[46] S. Liu, D. Brunel, K. Sun, Y. Xu, F. Morlet-Savary, B. Graff, P. Xiao, F. Dumur, J. Lalevée, A monocomponent bifunctional benzophenone–carbazole type II photoinitiator for LED photoinitiating systems, Polymer Chemistry, 2020, 11.21, 3551-3556.

[47] M. Abdallah, D. Magaldi, A. Hijazi, B. Graff, F. Dumur, J.P. Fouassier, T.T. Bui, F. Goubard, J. Lalevée, Development of New High-Performance Visible Light Photoinitiators Based on Carbazole Scaffold and Their Applications in 3D Printing and Photocomposite Synthesis, J. Polym. Sci., Part A, 2019, 57, 2081–2092.

[48] S. Liu, B. Graff, P. Xiao, F. Dumur, J. Lalevée, Nitro-Carbazole Based Oxime Esters as Dual Photo/Thermal Initiators for 3D Printing and Composite Preparation, Macromolecular Rapid Communications, 2021, 42.15, 2100207.

[49] S. Liu, N. Giacoletto, M. Schmitt, M. Nechab, B. Graff, F. Morlet-Savary, P. Xiao, J. Lalevée, Effect of Decarboxylation on the Photoinitiation Behavior of Nitrocarbazole-Based Oxime Esters, Macromolecules, 2022, 55.7, 2475-2485.

[50] F. Hammoud, N. Giacoletto, M. Nechab, B. Graff, A. Hijazi, F. Dumur, J. Lalevée, 5, 12-Dialkyl-5, 12-dihydroindolo [3, 2-a] carbazole-Based Oxime-Esters for LED Photoinitiating Systems and Application on 3D Printing, Macromolecular Materials and Engineering, 2022, 2200082.

[51] Z.H. Lee, S. C. Yen, F. Hammoud, A. Hijazi, B. Graff, J. Lalevée, Y.C. Chen, Naphthalene-Based Oxime Esters as Type I Photoinitiators for Free Radical Photopolymerization, Polymers, 2022, 14.23, 5261.

[52] F. Dumur, Recent advances on pyrene-based photoinitiators of polymerization, European Polymer Journal, 2020, 126, 109564.

[53] S. Telitel, F. Dumur, T. Faury, B. Graff, M. A. Tehfe, D. Gigmes, J.P. Fouassier, J. Lalevée, New core-pyrene π structure organophotocatalysts usable as highly efficient photoinitiators. Beilstein journal of organic chemistry, 2013, 9.1, 877-890.

[54] M. A. Tehfe, F. Dumur, B. Graff, F. Morlet-Savary, D. Gigmes, J. P. Fouassier, J. Lalevée, Design of new Type I and Type II photoinitiators possessing highly coupled pyrene–ketone moieties, Polymer Chemistry, 2013, 4.7, 2313-2324.

[55] J. V. Crivello, F. Jiang, Development of pyrene photosensitizers for cationic photopolymerizations, Chemistry of materials, 2002, 14.11, 4858-4866.

[56] M. V. Encinas, E. A. Lissi, C. Majmud, J. J. Cosa, Photopolymerization in aqueous solutions initiated by the interaction of excited pyrene derivatives with aliphatic amines, Macromolecules, 1993, 26.23, 6284-6288.

[57] A. Mishra, S. Daswal, Copolymerization of n-butylacrylate with methylmethacrylate by a novel photoinitiator, 1-(bromoacetyl) pyrene, International Journal of Chemical Kinetics, 2007, 39.5, 261-267.

[58] M. V. Encinas, C. Majmud, J. Garrido, E. A. Lissi, Methyl methacrylate polymerization photoinitiated by pyrene in the presence of triethylamine, Macromolecules, 1989, 22.2, 563-566.

[59] F. Dumur, Recent advances on anthracene-based photoinitiators of polymerization. European Polymer Journal, 2022, 111139.

[60] D. K. Balta, N. Arsu, Y. Yagci, S. Jockusch, N. J. Turro, Thioxanthone− anthracene: A new photoinitiator for free radical polymerization in the presence of oxygen, Macromolecules, 2007, 40.12, 4138-4141.

[61] D. T. Beyazit, B. Gacal, Y. Yagci, An amphipathic thioxanthone-anthracene photoinitiator for free-radical polymerization. Turkish Journal of Chemistry, 2013, 37.4, 525-537.

[62] J. V. Crivello, M. Jang, Anthracene electron-transfer photosensitizers for onium salt induced cationic photopolymerizations, Journal of Photochemistry and Photobiology A: chemistry, 2003, 159.2, 173-188.

[63] M. Rahal, H. Bidotti, S. Duval, B. Graff, T. Hamieh, J. Toufaily, F. Dumur, J. Lalevée, Investigation of pyrene vs Anthracene-based oxime esters: Role of the excited states on their polymerization initiating abilities, European Polymer Journal, 2022, 177, 111452.

[64] F. Dumur, Recent advances on visible light Phenothiazine-based photoinitiators of polymerization, European Polymer Journal, 2022, 110999.

[65] L. Deng, L. Tang, J. Qu, Novel chalcone-based phenothiazine derivative photoinitiators for visible light induced photopolymerization with photobleaching and good biocompatibility, Progress in Organic Coatings, 2022, 167, 106859.

[66] Z. Gomurashvili, J. V. Crivello, Monomeric and polymeric phenothiazine photosensitizers for photoinitiated cationic polymerization. Macromolecules, 2002, 35.8, 2962-2969.

[67] Z. Gomurashvili, J. V. Crivello, Phenothiazine photosensitizers for onium salt photoinitiated cationic polymerization. Journal of Polymer Science Part A: Polymer Chemistry, 2001, 39.8, 1187-1197.

[68] M. Rahal, M. Abdallah, T. T. Bui, F. Goubard, B. Graff, F. Dumur, J. Toufaily, T. Hamieh, J. Lalevée, Design of new phenothiazine derivatives as visible light photoinitiators. Polymer Chemistry, 2020, 11.19, 3349-3359.

[69] M. Li, B. Bao, J. You, Y. Du, D. Li, H. Zhan, L. Zhang, T. Wang, Phenothiazine derivatives based on double benzylidene ketone structure: Application to red light photopolymerization. Progress in Organic Coatings, 2022, 173, 107217.

[70] X. Peng, D. Zhu, P. Xiao, Naphthoquinone derivatives: Naturally derived molecules as blue-light-sensitive photoinitiators of photopolymerization, European Polymer Journal, 2020, 127, 109569.

[71] J. P. Fouassier, F. Morlet-Savary, J. Lalevée, X. Allonas, C. Ley, Dyes as photoinitiators or photosensitizers of polymerization reactions. Materials, 2010, 3.12, 5130-5142.

[72] F. Hammoud, A. Pavlou, A. Petropoulos, B. Graff, M.G. Siskos, A. Hijazi, F. Morlet-Savary, F. Dumur, J. Lalevée, Naphthoquinone-based imidazolyl esters as blue-light-sensitive Type I photoinitiators, Polymer Chemistry, 2022, 13, 4817-4831.

[73] G. Noirbent, F. Dumur, Recent advances on naphthalic anhydrides and 1, 8-naphthalimide-based photoinitiators of polymerization. European Polymer Journal, 2020, 132, 109702.

[74] P. Xiao, F. Dumur, M. Frigoli, M. A. Tehfe, B. Graff, J. P. Fouassier, D. Gigmes, J. Lalevée, Naphthalimide based methacrylated photoinitiators in radical and cationic photopolymerization under visible light. Polymer Chemistry, 2013, 4.21, 5440-5448.

[75] J. Yang, C. Xu, Y. Xiong, X. Wang, Y. Xie, Z. Li, H. Tang, A green and highly efficient naphthalimide visible photoinitiator with an ability initiating free radical polymerization under air. Macromolecular Chemistry and Physics, 2018, 219.24, 1800256.

[76] S. Liu, N. Giacoletto, B. Graff, F. Morlet-Savary, M. Nechab, P. Xiao, F. Dumur, J. Lalevée, N-naphthalimide ester derivatives as Type I photoinitiators for LED photopolymerization, Materials Today Chemistry, 2022, 26, 101137.